Research Square

Preprints are preliminary reports that have not undergone peer review.
They should not be considered conclusive, used to inform clinical practice,
or referenced by the media as validated information.

Ocean acidification and aragonite saturation compounding anthropogenic stressors on marine life

Howard Dryden

drydenaqua@me.com

Goes Foundation

Research Article

Keywords: ocean acidification, aragonite saturation state, winter exposure, ecological thresholds, calcifying plankton, pteropods, cumulative stressors, marine defaunation, regime shifts, net primary production

Posted Date: October 21st, 2026

DOI: https://doi.org/10.21203/rs.3.rs-11145455/v2

License: This work is licensed under a Creative Commons Attribution 4.0 International License.
Read Full License

Additional Declarations: The authors declare no competing interests.

Ocean acidification and aragonite saturation compounding anthropogenic stressors on marine life

Howard Dryden and Diane Duncan

GOES Foundation, Seahorse Point Nature Laboratory, Bocas del Toro, Panama

Correspondence to: Howard Dryden (howard@goesfoundation.com), ORCID: https://orcid.org/0000-0002-5068-2113

Telephone of corresponding author: +44 7748701275

Abstract

Background: Ocean acidification is usually reported as annual or global means, yet marine organisms respond to the saturation state they actually meet, which in cold and productive waters is the winter minimum. We recomputed the aragonite saturation state (Ω) of winter casts at carbonate time-series sites from the primary measurements and compared the mapped winter field of the OceanSODA-ETHZ product for 1982 to 2024 with an ecological reference threshold that falls smoothly with latitude.

Results: In the Iceland Sea, the subarctic North Pacific and the Southern Ocean, winter Ω already sits at or below 1.6, the threshold for sensitive aragonite calcifiers, and the Iceland Sea record declined by 0.0046 ± 0.0007 Ω per year before 2014. About 35% of the mapped ocean surface, carrying 46% of its net primary production, was below its winter threshold in 2022 to 2024, up from 18% in 1982 to 1984; the present share lies between 27 and 52% across the threshold choices tested, and extending each cell's 43-year trend carries it to about 45% by 2045. That water carries 59% of chlorophyll; it coincides with the high-latitude basins and the eastern tropical upwelling regions, where pteropods, bivalve larvae, oyster hatcheries and juvenile crabs already show responses at the levels now reached. A

documented index of published declines puts the loss of marine animal life since 1850 at about 46 to 65%, so acidification is acting on a system that fishing, whaling, habitat loss, pollution and climate disruption had already depleted.

Conclusions: We set out, as a testable hypothesis, how a falling pH may alter colloidal chemistry, micro-viscosity and iron availability, compounding the effects of aragonite solubility. Cutting carbon dioxide emissions and reducing harm will slow acidification but cannot reverse it, and because the marine system is already depleted, recovery may not be possible without active restoration. We conclude that ocean acidification should be treated as an active part of cumulative marine risk, that reporting should use winter minima alongside annual means, and that redox potential, zeta potential and particle measurements should be added to time-series stations.

Keywords: ocean acidification; aragonite saturation state; winter exposure; ecological thresholds; calcifying plankton; pteropods; cumulative stressors; marine defaunation; regime shifts; net primary production

1 Background

The aragonite saturation state, Ω, is calculated from measured properties of seawater, including the partial pressure of carbon dioxide, pH, total alkalinity, calcium concentration, salinity and temperature [1]. It describes how easily marine animals can build and keep shells and skeletons of aragonite, which is a form of calcium carbonate. Aragonite dissolves below Ω = 1, a shell forms readily above about Ω = 1.6, and sensitive calcifiers begin to

suffer in the marginal zone between those two values (Section 4.2). Aragonite saturation is not a simple water-quality parameter, because it has a profound influence on the physical and chemical structure of the water and on the behaviour of the organisms that live in it (Section 4.5).

Saturation is usually reported as an annual mean, and in cold water an annual mean is almost always higher than the winter reading that marine life actually encounters. The ocean acidification planetary boundary is a clear example, since it is expressed as a global annual mean of Ω 2.75, which is 80% of the pre-industrial value of 3.44 [2, 3]. That threshold was chosen to keep high-latitude surface water, the first to approach undersaturation, above the point of dissolution and to protect most coral systems. The difficulty is not that the framework ignores cold water, but that a single global annual mean cannot show when individual cold basins cross the line in winter. A recent reassessment raised the pre-industrial baseline to Ω 3.51, found that by 2020 the global mean had entered the uncertainty range of the 20% boundary and that four of seven ocean regions, the Arctic among them, had crossed the boundary, and argued for a stricter 10% boundary that the whole surface ocean passed by 2000 [4].

This study addresses two questions about the present state of the acidifying ocean. First, how much of the ocean already sits below the saturation at which its own calcifying organisms respond when exposure is judged at the winter minimum rather than the annual mean? Second, what state was marine life already in when that chemistry began to change? To answer the first question, we recomputed the winter casts of four long carbonate time series from the primary measurements, compared the mapped winter field of the

OceanSODA-ETHZ product [5] with an ecological reference threshold graded by latitude, and weighted the exposed water by satellite measures of its productivity. To answer the second question, we compiled the published record of marine animal declines since 1850 into an openly documented index. We then set out, as a clearly labelled hypothesis, how a falling pH may act on plankton through colloidal chemistry, viscosity and iron, beyond its effect on shells, and we report one satellite test of that hypothesis.

2 Methods

2.1 Data sources and their roles

Two kinds of measurement play fixed and separate roles throughout this study. The gridded OceanSODA-ETHZ product [5, 6] supplies the spatial and global evidence, because only a mapped field covers the whole ocean surface, while discrete ship-based casts supply independent regional validation and direct winter measurements at selected sites. Neither is used in the role of the other, and no global figure rests on the discrete sites alone. The discrete casts come from the SPOTS time-series synthesis [7], cross-checked against GLODAPv2.2022 [8] and CODAP-NA [9].

Table 1: Data sources used in this study

Dataset	Variable(s) used	Coverage	Source
OceanSODA-ETHZ v2025	omega_ar (aragonite saturation), omega_ar_uncert	1×1°, monthly, 1982–2024, global	Gregor & Gruber [5]; NOAA NCEI OCADS accession 0220059, https://doi.org/10.25921/m5wx-ja34; landing page: https://www.ncei.noaa.gov/access/metadata/landing-page/bin/iso?id=gov.noaa.nodc:0220059
SPOTS time-series synthesis	Dissolved inorganic carbon (DIC), total alkalinity, pCO_2, temperature, salinity, silicate, phosphate (discrete casts)	Iceland Sea, Irminger Sea, Station K2, Munida	Lange et al. [7]
GLODAPv2.2022	Interior/surface DIC, total alkalinity, nutrients (quality-control cross-check for discrete casts)	Global ocean interior compilation	Lauvset et al. [8]
CODAP-NA	Discrete inorganic carbon, oxygen, and nutrients (North American margin cross-check)	North American ocean margins	Jiang et al. [9]
MODIS-Aqua Kd490 and chlorophyll-a (Station ALOHA optics)	Diffuse attenuation coefficient Kd490 and chlorophyll-a (Section 2.7, Station ALOHA)	4 km monthly, 2003–2021, box of 6° latitude by 8° longitude around Station ALOHA	NASA OBPG R2018.0 products served by NOAA OceanWatch ERDDAP (aqua_kd490_monthly_2018_0, aqua_chla_monthly_2018_0)
ESA Ocean Colour CCI v6.0	Total absorption coefficient at 443 nm (Section 2.7, Station ALOHA)	4 km annual, 1998–2025, Station ALOHA box	Plymouth Marine Laboratory THREDDS server (oceancolour.org), which serves the v6.0 processing beyond the 2022 end of the archived release
MODIS-Aqua net primary production (erdMH1ppmday)	Net primary production, mg C m^{-2} d^{-1} (Section 2.5; weighting of the winter field)	4 km monthly, January 2019 to December 2021 (34 months available), global	NASA OBPG, Behrenfeld–Falkowski vertically generalised production model [126], served by NOAA CoastWatch ERDDAP; product marked experimental
MODIS-Aqua particulate inorganic carbon (erdMPICmday) and chlorophyll-a (erdMH1chlamday)	Surface calcite concentration, mol m^{-3} [127]; chlorophyll-a, mg m^{-3} (Section 2.5)	4 km monthly, January 2019 to December 2021 (36 and 35 months), global	NASA OBPG R2022 and R2018 products served by NOAA CoastWatch ERDDAP

Every primary dataset used in this study, with the variables taken from it, its coverage and its accession or citation; all of these datasets are public.

2.2 Carbonate chemistry of the discrete casts

The aragonite saturation state of the discrete casts was computed with PyCO2SYS v1.8 [10] from the primary SPOTS measurements [7]. Dissolved inorganic carbon was paired with measured total alkalinity where alkalinity exists, from 2014 onwards, and with the partial pressure of carbon dioxide (pCO_2) for the Iceland Sea and Irminger Sea records before 2014, when alkalinity was not measured at those stations. Every calculation used measured in-situ temperature, salinity, silicate, phosphate and pressure, the constants of Lueker et al. [11], Dickson [12] and Uppström [13] on the total pH scale, and samples from the shallowest 25 dbar, about 25 m depth (Additional file 1, Table S1). The two input pairs give Ω values that are not fully consistent, and the disagreement is largest in cold water [14, 15], so the step at 2014 in Figure 1 is a change in the analysis rather than in the ocean, and no slope is fitted across that change. Winter is taken as January to March in the Northern Hemisphere and July to September in the Southern Hemisphere.

From 1995 the archived pCO_2 at these stations appears to be reported at a fixed laboratory equilibration temperature of 4 °C rather than at in situ temperature, and treating that value as the measurement temperature introduced a spurious step at 1995 of about +0.28 Ω in the Iceland Sea and −0.22 Ω in the Irminger Sea. The stored-sample protocol introduced in mid-1993 is described by Ólafsson et al. [16], and the interpretation of 4 °C is inferred from internal evidence (Additional file 1, Note S1). Taking the archived value at in-situ temperature removes the step and brings the implied alkalinity into agreement with the

alkalinity measured from 2014, with an alkalinity-to-salinity ratio of 65.9 against a measured 65.7. The corrected casts also lie within about 0.12 Ω of the independent gridded field in every period. Trends before 2014 were fitted by least squares against time alone and, for comparison with the published record, by multivariate regression on time and temperature, and the results do not change when the surface layer is taken as the shallowest 10 to 30 dbar (about 10 to 30 m) instead of 25 dbar.

2.3 A graded ecological reference threshold

A single threshold cannot serve every ocean, because the saturation state that an organism meets depends on temperature, and coral reefs and polar pteropods respond at very different values. The simplest scheme uses three fixed latitude bands (Ω 1.6 poleward of 50°, 2.4 between 30° and 50°, and 3.3 equatorward of 30°). A stepped scheme holds each threshold at its full value up to the band edge, so that open subtropical ocean between 20° and 30°, where no reefs grow, is judged against the reef value of 3.3. We therefore use a threshold that varies continuously with latitude. The cold-water end, Ω 1.6 poleward of 60°, sits just above the range of about Ω 1.2 to 1.5 in which bivalve larvae show a response [17] and pteropods are considered to be negatively affected [18], and matches the low saturation already measured in these waters [19]. The warm-water end, Ω 3.3 equatorward of 10°, is the saturation at which net carbonate accretion on reefs approaches zero [20]. Between 10° and 60° the threshold falls linearly with absolute latitude. Only the two ends rest on measured responses; the values between them are interpolation, and the latitudes over which the fall occurs are a stated choice whose effect we report. The ramp from 10° to

60° is the reference case. Two alternatives, a ramp from 20° to 60° and a ramp from 30° to 50°, give the structural range, and moving the warm-water end to Ω 3.0 or 3.6 gives the sensitivity to that value. The three-band scheme is reported once, in Section 3.2, to show what the graded threshold changes.

2.4 Winter threshold analysis and projections

The winter field was built from the OceanSODA-ETHZ aragonite saturation [5] as the February value north of the equator and the August value south of the equator for each of the 43 years from 1982 to 2024 on the native 1° grid, and the mean of the 2022–2024 winters is the reference present state. The main analysis uses the single coldest month because it classifies exposure, the saturation that an organism meets at the seasonal minimum, rather than fitting a trend. As a sensitivity test, we repeated the classification with the mean of the three winter months (January to March in the north, July to September in the south) in place of the single coldest month, which lowers the share of the ocean below its threshold from 35.1% to 34.4%, and changes the share at each projected date by 0.3 percentage points or less. Two further checks are given in Additional file 1, Table S2: taking each cell's own lowest month of the 2022–2024 monthly climatology in place of the fixed winter month gives 37.5%, and shifting the whole field by 0.1 Ω, the size of the systematic differences between the mapped product and the discrete casts (Section 2.2), moves the present share to 41.8% if the field is lowered and 29.4% if it is raised. The same classification applied to the 1982–1984 winters gives the change over the record (Section 3.2).

A linear trend was fitted in every cell by ordinary least squares against year, using 43 points per cell and excluding cells with any missing winter value. The projections to 2035, 2045 and 2055 apply that trend to the reference field over 12, 22 and 32 years, counted from 2023, the centre of the reference period. Cells with no complete 43-winter series, 2,101 cells or 2.5% of the mapped area, almost all seasonally ice-covered polar water, have no fitted trend and cannot be projected. In the projections these cells are counted as not below their threshold, although their area stays in the total, and 1,940 of them are already below their threshold, so the projected shares are about 2.3 percentage points low; we also report the shares with those cells held at their present state. Areas are weighted by the cosine of latitude in every calculation of this kind.

2.5 Weighting the winter field by productivity

To ask how much of the ocean's productive base lies in water below its winter threshold, rather than how much of its area, each 1° cell of the winter field was weighted by three satellite measures of the productive base of the food web: net primary production from the Aqua MODIS vertically generalised production model [126], surface calcite concentration from MODIS particulate inorganic carbon [127], and surface chlorophyll-a (Table 1). Each weight is the mean of the monthly values available from January 2019 to December 2021 of a 1° block mean of the 4 km product, estimated from a regular subset of 36 of the 576 pixels in each cell and used only when at least 18 of the 36 were valid. Pixel values of production above 10,000 mg C m^{-2} d^{-1} (0.58% of valid pixels) were treated as retrieval errors and removed, and calcite values above the product's stated valid maximum of 0.125

mol m^{-3} (0.017%) were removed. The weighted share is the weighted area below threshold divided by the weighted area of all mapped cells with a valid weight (99.8 to 99.9% of the mapped area); the area share on those same cells differs from the all-cell area share by no more than 0.1 percentage point. The ratio of a weighted share to the area share equals the mean weight of the exposed cells divided by the mean weight of all mapped cells. These weights describe where production, calcite and chlorophyll sit relative to the winter chemistry; they are proxies for the productive base of the food web, not measurements of animal biomass, and they are annual means, whereas the saturation state is a winter value. Poleward of 60°, no satellite value exists in the winter months, so the weights there are means of the summer months; we therefore also report the production-weighted share with the missing months counted as zero production and with those cells left out. Because the weights are annual means, we repeated the calculation month by month, comparing each calendar month's saturation state (mean of 2022 to 2024) with the threshold and weighting each cell by the satellite value for that month (Additional file 1, Figure S2).

2.6 Statistical analysis and uncertainty

Three independent sources of uncertainty were quantified for the percentage of mapped ocean below its graded threshold. Measurement uncertainty was propagated from the product's own per-cell reported uncertainty by Monte Carlo simulation, using 500 Gaussian perturbations of the 2022–2024 mean field; this treats the errors of neighbouring cells as independent, so a systematic offset of the whole field is tested separately (Section 2.4). Spatial sampling uncertainty was obtained by a block bootstrap of 10° by 10° blocks with

5,000 resamples, so that spatially correlated neighbouring cells are not treated as independent evidence. Structural uncertainty is the range across the three ramp positions of Section 2.3, the widest of the three tiers; the sensitivity to the warm-water end of the threshold is wider still, and the range across both is the one quoted in the Abstract (Section 3.2). Per-cell winter trends were tested against a null slope of zero, and significance was also assessed on a spatially thinned subsample of every fifth cell in latitude and longitude, which gives 1,329 quasi-independent cells at roughly 5° spacing, with a Wilcoxon signed-rank test of the median trend. The per-cell significance tests do not correct for autocorrelation within each winter series; the spatially thinned Wilcoxon test is the test we rely on. Point estimates are quoted to one decimal place in the Results and tables, and percentages are rounded to the nearest whole point in the Abstract, Discussion and Conclusions and where a range is given. The whole classification pipeline was independently re-implemented and reproduces every reported point estimate exactly.

2.7 The colloidal-chemistry hypothesis and its test at Station ALOHA

Aragonite saturation is more than a measure of the solubility of calcium carbonate. It is set by pH, alkalinity and the carbonate buffer, so a change in saturation signals a change in the chemistry of the water and in the conditions for the organisms that live in it. The hypothesis that we set out in Section 4.5 and test in part here is that a falling pH and the loss of buffer capacity make dissolved organic matter and fine particles coagulate and flocculate more readily, which raises the colloidal load and the effective viscosity at the scale of small organisms and particles, the micro-viscosity. These changes could darken the

water, favour small phytoplankton and slow microzooplankton and larval stages, and, once a trigger such as eutrophication or heat has started the cascade, contribute to the spread of dead zones and to regime shifts.

The colloidal chemistry cannot be measured at the scale of the ocean, because no sustained observing programme records redox potential, zeta potential or particle size, but the hypothesis makes one prediction that satellites can test: the water should become less transparent without a matching rise in chlorophyll or in coloured dissolved organic matter. We report that test because it is the only part of the hypothesis that existing public records can address, and we treat it as exploratory: it can show that the prediction is not contradicted, not that the mechanism operates. We examined satellite optics at Station ALOHA, an oligotrophic site in the North Pacific subtropical gyre where surface chlorophyll shows no trend in three decades of water samples [21]. Monthly 4 km products of the diffuse attenuation coefficient Kd490 and of chlorophyll-a from MODIS-Aqua (NASA R2018.0, served by NOAA OceanWatch ERDDAP) were averaged as geometric means over a box of 6° latitude by 8° longitude around the station, using all months. Trends over 2003 to 2021 were fitted by ordinary least squares, with p values corrected for first-order autocorrelation. Total absorption at 443 nm was taken for the same box from the ESA Ocean Colour CCI v6.0 annual product of inherent optical properties over 1998 to 2025 (the v6.0 processing, which the Plymouth Marine Laboratory server extends beyond the 2022 end of the archived release). Satellite attenuation and chlorophyll are derived from the same blue-green reflectance ratio, so attenuation adds information only where it departs from chlorophyll, and for that reason the test uses a site with no chlorophyll trend.

2.8 Biocurve construction

No census of global marine animal life exists, either for today or for 1850, and none is in prospect. We therefore built an openly documented index, the biocurve, as a weighted mean of the fraction of each animal group remaining against an 1850 baseline of 100%, $\text{Nature}(t) = \Sigma(w_i \cdot r_i) / \Sigma w_i \times 100\%$, with every r_i equal to 1 in 1850. Thirteen groups enter with the importance weights and documented fractions listed in Additional file 1, Table S4, and each fraction is referenced to its published source in Table 2. The importance weighting gives most weight to apex, structural and calcifying groups, and equal weights and a production weighting were computed as alternatives (Additional file 1, Table S5). The index covers animal life in the upper 200 m and excludes the mesopelagic zone, an exclusion that runs in one direction, because counting the deep layer would raise the index.

The 1850 value is definitional, and the present value is the only point computed directly from data. The 1900, 1950 and 1985 values are an interpolation positioned by the periods of the documented declines, drawn from 1950 as $R(t) = 69 - 33.6 \times ((t - 1950)/73)$ raised to the power 1.4, in which the exponent is a stated choice. Groups whose records begin after 1850 are treated as though their published decline were the whole decline, so the index overstates what remains and should be read as an upper bound on surviving structure. The full construction and its sensitivity tests are given in Additional file 1, Note S3.

2.9 Grading of evidence

Because the argument combines measurement, established chemistry and inference, we grade every claim in four tiers. Established claims rest on direct measurement or on chemistry that is not in dispute. Demonstrated claims are shown in engineered seawater systems but not yet at the scale of the ocean. Hypothesised claims follow from established chemistry but have not been observed in the open ocean. Scenarios follow from ecological theory rather than from measurement, and they are labelled as scenarios wherever they appear.

2.10 Use of artificial intelligence

The authors used Claude (Anthropic), a large language model, as an assistant for compiling published values, processing the OceanSODA-ETHZ and SPOTS data, recomputing the carbonate system, preparing figures and checking consistency. Numeric claims were checked against their primary sources or re-derived from the primary data, a consistency audit before this revision corrected the discrepancies that it found, and the authors directed, verified and approved all analyses and conclusions and take full responsibility for the content of this study.

3 Results

3.1 Winter saturation at the cold-water time-series sites

The Iceland Sea holds the longest carbonate record of the cold-water basins considered here. Ólafsson et al. [22] measured a decrease in winter surface Ω of 0.0072 ± 0.0007 per year between 1985 and 2008, with winter surface pH falling by 0.0024 ± 0.0002 units per year. The OSPAR assessment [23] extends these results, with an Iceland Sea trend of about 0.006 Ω per year over 1985 to 2020 and an Irminger Sea trend of about 0.012 Ω per year over 1983 to 2020. It records Iceland Sea Ω at or around 1.5 in the 1980s, with seasonal minima reaching about 1.3 since 2015, while the Irminger Sea has only started to reach values below 1.5 seasonally over the past decade.

Over the internally consistent record before 2014, the recomputed Iceland Sea winter series declines at −0.0046 ± 0.0007 Ω per year on a simple fit against time ($n = 57$, $p < 10^{-8}$), while the Irminger Sea is statistically flat over the same period (−0.0014 ± 0.0009 Ω per year, $n = 51$, $p = 0.13$; Figure 1). The Irminger record is flat over this period on the simple fit, whereas the OSPAR assessment reports a decline [23]; the difference arises from the period, from the temperature adjustment, and from the reporting temperature of the archived carbon dioxide values before 2014 (Section 2.2). The contrast between the two stations shows that the fitting method does not manufacture declines, so the significant trend in the Iceland Sea belongs to the water rather than to the method. With the multivariate regression on time and temperature, the recomputed 1985–2008 casts reproduce the published temperature-adjusted Iceland Sea trend of −0.0072 ± 0.0007 Ω

per year [22] at −0.0059 ± 0.0010 Ω per year, which agrees within about two combined standard errors (Additional file 1, Note S1).

Of the four cold-water basins, the Iceland Sea, the subarctic North Pacific and the Southern Ocean already sit at or below Ω 1.6 in winter, while the warmer Irminger Current water sits just above that threshold. The subantarctic site at Munida, off New Zealand, reads about Ω 2.0 in water about 9 °C warmer than the polar sites, which is consistent, within the spread of the neighbouring mapped cells (1.93 to 2.61), with the relation across those cells of about 0.08 Ω per degree Celsius (Additional file 1, Note S1). Station K2 and Munida have too few winter casts to support a fitted trend, so their long-term rates come from the mapped product [24, 25] (Additional file 1, Table S3).

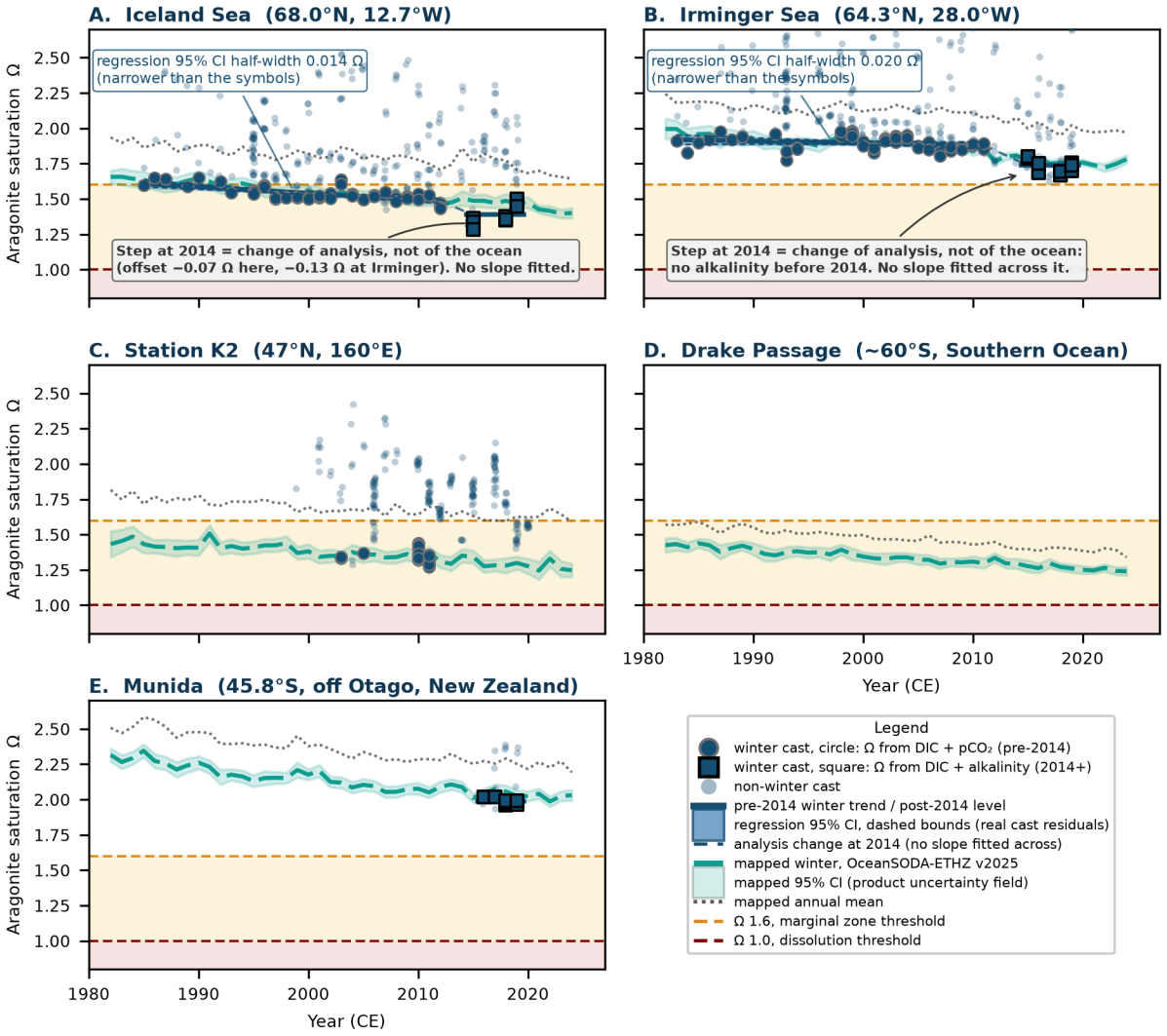


Figure 1: Measured winter surface aragonite saturation at five subpolar and high-latitude sites

Panels show the Iceland Sea (A), the Irminger Sea (B), Station K2 (C), Drake Passage (D) and Munida (E). Circles show discrete winter casts before 2014, computed from dissolved inorganic carbon with the partial pressure of carbon dioxide; squares show casts from 2014 onwards, computed from dissolved inorganic carbon with measured alkalinity. Dark blue shows the winter regression before 2014 with its 95% confidence band and the mean level after 2014; no slope is fitted across 2014 because the change of input pair introduces an analytical offset. Teal dashed lines show the mapped OceanSODA-ETHZ winter mean with its 95% band [5], grey dotted lines show the mapped annual mean, and faint small circles show casts outside winter. Winter is January to March in the Northern Hemisphere and July to September in the Southern Hemisphere. Drake Passage has no sustained discrete record, so only the mapped product is shown there. Methods and cast counts are given in Additional file 1, Note S1.

3.2 Share of the winter ocean below its ecological threshold

On the graded threshold, 35.1% of the mapped ocean surface was below its winter threshold in the 2022–2024 winters (Figure 2). On the same cells, 18.1% was below its threshold in the 1982–1984 winters, so the share has nearly doubled over the 43-year record (Additional file 1, Table S2 gives the intermediate periods). Weighting each cell by the satellite measures of the productive base of the food web raises the share to 46.2% for net primary production, 51.0% for calcite and 58.7% for chlorophyll (Table 3; Section 3.3), so the water below its threshold holds more of that base than its share of area.

Table 3: Share of the mapped ocean below its winter threshold, by area and by satellite weights

Measure	Share below threshold	Ratio to area share
Area (aragonite saturation)	**35.1%**	**1.00**
Net primary production	**46.2%**	**1.32**
Calcite (particulate inorganic carbon) concentration	**51.0% (51 to 61% across variants)**	**1.45**
Chlorophyll-a	**58.7%**	**1.67**

Winter 2022 to 2024; graded threshold, ramp from 10° to 60°. Weights are 2019 to 2021 means (Section 2.5), summer means poleward of 60°, and are proxies for the productive base of the food web, not animal biomass; the ratio is the weighted share divided by the area share. Counting the unmeasured polar winter months as zero production gives 40.3% for net primary production (Section 3.3).

The share depends mainly on where the threshold is set: it is between 35 and 50% for the three ramp positions and between 27 and 52% for a warm-water end of Ω 3.0 or 3.6 (Additional file 1, Table S2, which also gives the Monte Carlo and block-bootstrap intervals). The three-band scheme gave 43.7%, of which the 20° to 30° band accounts for 7.1 of the 8.6 points (Section 2.3).

Extending each cell's own 43-year trend, an estimated 39% will be below its threshold by 2035, 45% by 2045 and 52% by 2055 (41%, 48% and 54% with the cells without a fitted trend held at their present state). Most of the increase arises equatorward of 40°, where the threshold is the interpolated or reef-anchored part of the ramp, because the polar water is already below its threshold.

Poleward of 50°, 91.5% of the area is already below its threshold, and poleward of 60°, the share is 88.0%, so that water would have been below for more than a decade by 2035 if its present state persisted, which the negative trends make likely.

Winter saturation declined in almost every cell of the ocean from 1982 to 2024. In the thinned subsample, 99.8% of cells show an individually significant negative trend ($p < 0.05$), and a Wilcoxon signed-rank test rejects a zero median trend ($p < 0.001$). The area-weighted mean trend is −0.073 Ω per decade, and the median is −0.072 Ω per decade, consistent with the global trend of −0.071 ± 0.006 Ω per decade over 1982 to 2021 that Ma et al. [26] obtained from an earlier version of the same product.

The water below its threshold is not randomly distributed across the ocean surface. Seventy-one per cent of it lies poleward of 40°, including nearly all of the Southern Ocean and the subarctic North Pacific, and most of the rest lies in the eastern tropical Pacific, in the equatorial cold tongue and along the Peru–Chile margin, with parts of the California Current and the Benguela system, while the subtropical gyres remain above threshold. The two persistent high-nutrient, low-chlorophyll regions in the Southern Ocean and the subarctic North Pacific lie within this low-saturation water, where iron deficiency limits primary production and leaves nutrients unused [27, 28].

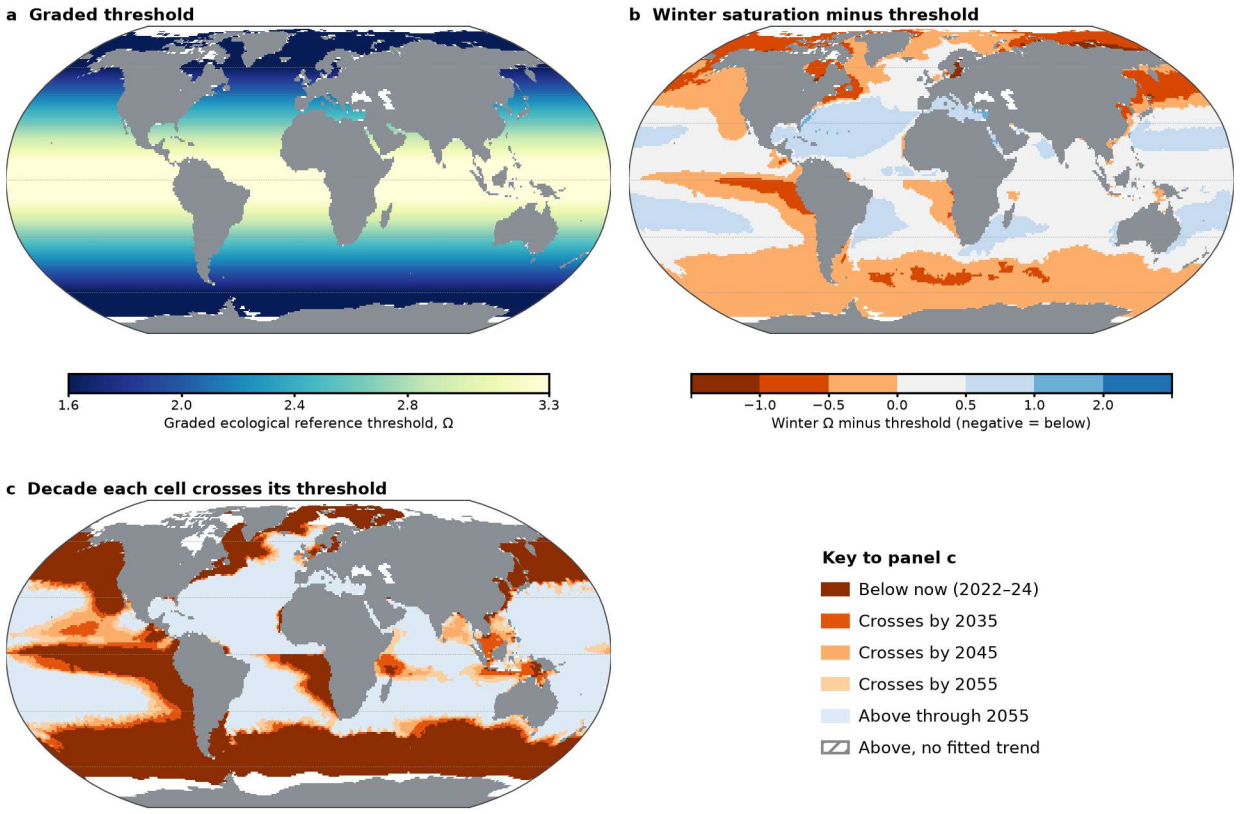


Figure 2: Winter surface aragonite saturation compared with a graded ecological reference threshold

(a) The threshold falls linearly with absolute latitude from Ω 3.3 equatorward of 10° [20] to Ω 1.6 poleward of 60° [17–19]. (b) Winter saturation in the 2022–2024 winters minus the threshold; orange-to-brown cells are below threshold. (c) The decade in which each cell crosses its threshold on its own 1982–2024 winter trend [5], from below threshold now (darkest) to above threshold through 2055 (palest); cells above threshold with no fitted trend are hatched. Winter is February in the Northern Hemisphere and August in the Southern Hemisphere. Land is grey; cells without winter data (mainly sea ice) are white; where adjacent polar water is measured, its median Ω is about 1.4, even in summer. Projections are linear and should be read as indicative beyond about 2045.

3.3 Productivity of the water below its threshold

Per unit of area, the water below its threshold has about 1.3 times the annual-mean production of the ocean average (639 against 484 mg C m^{-2} d^{-1}). The production-weighted share exceeds the area share under every ramp position and at both alternative warm-water ends, and its block-bootstrap interval is 41.7 to 50.7%. Poleward of 60°, the weights are summer means; counting the missing polar months as zero production lowers the share to 40.3% (ratio 1.15), and leaving those cells out raises the ratio to 1.36, so the ratio lies between 1.15 and 1.36 depending on how polar winter is treated. Matching each calendar month's saturation state to that month's production gives a smaller but still positive association (ratio 1.18, at or above 1 in eleven of the twelve months; 1.09 with winter-month weights alone; Additional file 1, Figure S2), and judged on the summer saturation state, the ratio is 0.98, so the association belongs to the winter state that calcifiers must survive. The calcite share is the least secure of the three: the 100 cells with the largest calcite weight hold 21% of the total, and almost all lie within 300 km of land.

3.4 Documented declines and the biocurve

Table 2 lists the documented declines in marine animal life and calcifiers since 1850, each a published measurement or indicator. The largest losses are among the large animals, since wild marine mammals [29], exploited fish [30, 31], oceanic sharks and rays [32] and monitored seabirds [33] have each lost between about one half and about 70%, and coral reefs [34], North Atlantic krill [35] and marine vertebrates in the Living Planet Index [36] also show declines.

Table 2: Documented declines in marine animal life and calcifiers since 1850

Species / group	Approx. location	Time frame	Documented change (loss of nature)	Biocurve value at end of record (% of 1850)†	Reference
Predatory fish (trophic level ≥3.5)	Global	1880–2007	−67% (two-thirds)	45	[31]; cf. [37]
Planktonic foraminifera (calcite)	Global (Challenger→Tara)	1870s–2011	Shells are thinner in every modern specimen: 48–76% in N. dutertrei, up to ~30% in G. ruber (4 scans, eastern equatorial Pacific, 1875 vs 2011).	43	[38]
Coral reefs (coverage, biodiversity, catch per effort)	Global tropics	1950s–2015	Cover ~−50%; biodiversity −63%; catch per unit effort −60%	40	[34]
Exploited fish biomass (10 g–100 kg)	Large marine ecosystems	pre-industrial–1990s	To ~47% of pre-industrial (roughly halved)	52	[30]
Antarctic krill	SW Atlantic, Southern Ocean	1976–2003	38–81% per decade reported; contested (no significant decline from 1976 to 2016).	48	[39, 40]; cf. [41]
Krill (euphausiids)	North Atlantic (subpolar)	1958–2017	−50%	39	[35]
Coccolithophore calcification	Gulf of Maine	2001–2018	0.4→0.2 mg C m^{-3} d^{-1}, ~−50% over 2001–2018 (coincides with a water-mass change and rising Ω; not attributed to acidification)	39	[42, 43]
Pteropods (habitat suitability)	California Current System	1984–2019	Modelled exposure to Ω < 1.5 water rose 9% → 49% (hindcast indicator)	38	[18]
Wild marine mammals	Global	1850–2020	To ~30% of 1850 (−70%)	37	[29]
Marine vertebrates (Living Planet Index)	Global	1970–2020	−56%, 1970–2020 (contested)	37	[36]; cf. [44]
Snow crab	E. Bering Sea	2018–2021	> 10 billion lost (starvation after marine heatwave)	37	[45]
Oceanic sharks & rays	Global	1970–2018	−71%	39	[32]
Seabirds	Global	1950–2010	−70% (monitored populations)	43	[33]
Coastal & estuarine systems	12 estuarine/coastal systems	historical–late 20th C	>90% of formerly important species depleted, >65% of seagrass and wetland habitat destroyed; oyster reefs −85% globally [46].	49	[47]

Every row reports a published measurement or indicator; the foraminifera, coccolithophore and pteropod rows are calcification or habitat-suitability indicators rather than abundance counts, and contested figures are cited with their counter-evidence. The fifth column gives the whole-ocean biocurve value (Section 2.8) at the date the record ends, not a property of that group. † The biocurve value is the weighted mean of the fraction of

412 the 1850 level remaining across all documented groups (Additional file 1, Note S3), plotted
413 in Figure 3.

414 On the importance weighting, the biocurve stands at 35.4% of the 1850 level in about 2023
415 (a loss of about 65%), with a band of 28.5 to 44.7%; it is 48% with equal weights and 54%
416 on a production weighting (Figure 3; Additional file 1, Table S5). The spread between those
417 weightings reflects a real feature of the ocean, which now holds more raw weight of life
418 than working structure, because the dominant zooplankton pool has declined by about half
419 while apex and structural groups have lost two-thirds to three-quarters. The present value
420 is the only point computed from data, and the curve drawn back to 1850 uses a chosen
421 exponent of 1.4 (Section 2.8). That choice matters little: with any exponent from 1.2 to 1.8,
422 or with a straight line in place of the curve, the 1985 value lies between 53 and 60%,
423 against 57% on the curve used. The coastal and estuarine compartment pulls the index
424 down: leaving it out and rescaling the remaining weights to 100% raises the present value
425 from 35.4% to 38.5%, a loss of about 62% instead of 65%.

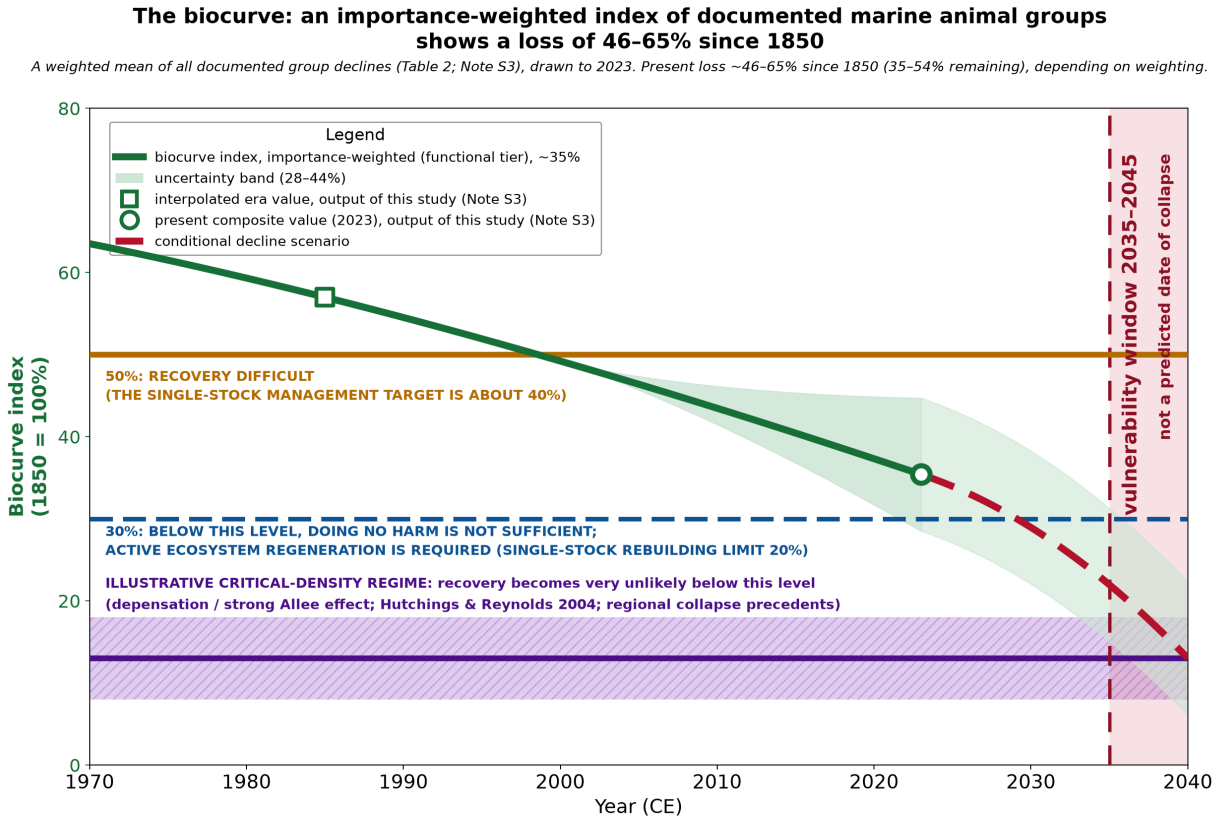


Figure 3: The biocurve, an index of documented declines in marine animal life since 1850

The index is expressed relative to its 1850 level of 100% and is drawn to about 2023 (Table 2; Additional file 1, Note S3) and is shown from 1970. The solid amber line at 50% and the dashed blue line at 30% are reference levels drawn by analogy with single-stock fisheries management, in which the target is the biomass at maximum sustainable yield, of the order of 40% of the unfished level, a stock below 20% must have a rebuilding plan, and one below 10% is considered for closure [133]; collapsed stocks rarely recover without such a plan [120, 121], and recovery becomes slower and less predictable the longer and deeper the depletion [134]. Below the first line, recovery becomes difficult, and below the second, doing no harm is not sufficient, and active ecosystem regeneration is required. The index is a composite of many groups, so the analogy is illustrative, and both lines are set above the single-stock values because the index includes slow-recovering groups. The curve is an interpretive synthesis rather than a census: the open square marks the interpolated value for 1985, the open circle marks the present composite, and the shaded band carries the uncertainty of the importance weighting. The red line is a scenario rather than a projection: it shows the direction that the theory of Section 4.6 permits if present pressures continue, and its entry into the illustrative critical-density regime (purple) is a stated choice rather than a computed value. The vertical band from 2035 to 2045 marks the period in which 39

to 45% of the mapped ocean is projected to be below its winter threshold (Figure 2); it is not a predicted date of collapse.

3.5 Light attenuation at Station ALOHA and the predictions of the hypothesis

At Station ALOHA, light attenuation in the MODIS-Aqua record rose by 3.1% over 2003 to 2021 ($p = 0.002$), while chlorophyll did not change significantly (+2.1%, $p = 0.61$), and the chlorophyll change accounts for about one-fifth of the rise in attenuation. The merged ESA record shows no trend in total absorption at 443 nm at this site over 1998 to 2025, so coloured dissolved organic matter is not the cause of the darkening, and particulate backscatter is the only optical term that rose, although that rise is not itself statistically significant. A small change in attenuation at the surface compounds through the water column, and the fitted rise removes about 4% of the light at 50 m, 8% at 100 m and 11% at 150 m.

The optical result is the first observable consequence that the hypothesis predicts: a rise in light-scattering particles without a matching rise in chlorophyll or in dissolved organic matter. It does not identify the particles, which could be colloidal matter formed by coagulation or small cyanobacteria (Section 4.5). The other predictions are untested in this study: that a higher micro-viscosity favours small phytoplankton and slows microzooplankton and larvae, and that more coagulation lowers the iron available in the high-nutrient, low-chlorophyll regions. The only existing observation points the other way, since chlorophyll in those regions has risen at the poles since 2010 [28], so the prediction of lower production there is not yet supported.

4 Discussion

4.1 Winter exposure and the limits of annual means

Biological thresholds are point-exposure relationships between the saturation that an organism meets and its response, so the quantity to compare with them is the saturation actually experienced, which in cold basins is the winter minimum, and an annual mean understates exposure. The point is practical rather than technical, because the change from one season to the next in these basins is as large as the underlying trend over several decades. In the Iceland Sea, the fitted trend explained 89% of the variance of the winter pH series but only 38% when all seasons were combined [22].

The measured winter state agrees with the wider literature on surface saturation. Poleward of about 60° north and south, many areas have surface Ω below 1.5, while between 40°N and 40°S the surface stays above 2.0 [48]. The Southern Ocean is the front line, where a shallow saturation horizon is projected to emerge suddenly this century [49, 50], shell dissolution is already observable in polar and upwelling waters [19, 51], and live pteropods have been observed to dissolve as Ω approaches 1.0 [52].

The coincidence of low saturation with productive water (Section 3.2) reflects one mechanism rather than chance, because upwelled deep water supplies both the nutrients that make these regions productive and the respired carbon dioxide that lowers their saturation. In the open equatorial upwelling, water below Ω 3.3 indicates this coupling rather than direct harm to reefs, which are coastal. The subpolar North Atlantic also holds the one region that has cooled while the rest of the ocean warmed, a pattern attributed to a

weakening of the overturning circulation [53], and colder water sits at lower saturation, so part of the low baseline of that region is thermal. The anomaly extends well below the surface layer [54], which matters for the many plankton that spend the daylight hours in deeper, colder and more corrosive water that no surface product records.

4.2 Biological thresholds and calcifier responses

The link between reduced calcification and falling saturation has been recognised since Kleypas et al. [55], and the dissolution point, Ω = 1.0, is not in dispute. In the California Current System, a strong upwelling region, a model hindcast shows the exposure of shelled pteropods to water below Ω 1.5 rising from 9% to 49% between 1984 and 2019 [18]. The measured biology matches that exposure, since 53% of pteropods sampled onshore show severe shell dissolution, against 24% offshore, in proportion to the undersaturated fraction of the water column [51]. When the same corrosive upwelled water entered Pacific Northwest oyster hatcheries from 2007, larval survival tracked the saturation of the intake water so closely that the industry now buffers and treats its seawater before use [56]. This evidence supports the use of Ω 1.6 as the cold-water end of the graded threshold in Figure 2.

Reef corals decline at a much higher saturation, with net carbonate accretion approaching zero around Ω 3.3 [20], which is the warm-water end of the graded threshold. Reefs cover less than 0.2% of the sea floor yet shelter about a quarter to a third of all marine species [136], so that end of the threshold carries an importance out of proportion to its area. Reefs nonetheless occupy only a small fraction of the tropical band, so the threshold between the

two ends describes a gradient of community sensitivity with temperature rather than a measured value. About a quarter of the sea-floor calcifiers studied already live in water that is undersaturated for their own skeletal mineral [57], and some authors contend that Ω is a proxy for the true driver, the ratio of bicarbonate to hydrogen ions [58].

Skeletal mineralogy sets the likely order in which calcifying groups become vulnerable. The modern ocean is a high-magnesium aragonite sea, with a molar magnesium-to-calcium ratio of about 5.2, near the highest of the past 250 million years [59, 60], and a calcium content of about 10 mmol kg^{-1}, less than half of the Cretaceous value [61]. High-magnesium calcite, used by coralline algae and sea urchins, dissolves more readily than aragonite, and aragonite dissolves more readily than low-magnesium calcite [62, 63]. The expected order is therefore high-magnesium calcite builders first, aragonite builders next, and calcite-shelled plankton last. We offer that order as a mechanistic expectation rather than a fitted relationship, because physiology often overrides mineralogy, and some species calcify more under elevated carbon dioxide [63]. The present fall in saturation is faster than in any past carbon-release event of the last 300 million years (the end-Cretaceous impact aside), because carbon dioxide is now released faster than in any of them [128]. We do not claim that the present level is the lowest of that record; the novelty lies in the rate, and the fall shows no sign of reversing, since every winter trend measured in this study is negative (Additional file 1, Table S3).

Calcium and magnesium, the divalent cations that help to set the saturation state of aragonite, also govern the coagulation and flocculation of colloids in seawater (Section 4.5). The magnesium-to-calcium ratio of seawater has risen from about 2 in the early Cenozoic

to its present value, a state last held around the Permian [59, 60]. Global temperatures are now among the lowest of the last quarter of a billion years [129], the buffer capacity of surface seawater is falling (Section 4.5), and anthropogenic emissions exceed 10 gigatonnes (Gt) of carbon per year [130]. Taken together, these conditions suggest that the importance of the aragonite index and the fragility of the marine ecosystem on which much of life on Earth depends may not have been fully appreciated.

A threshold alone cannot capture the whole biological risk, because harm also depends on the duration of exposure and on the life stage exposed. Bednaršek et al. [19] project pteropod shell dissolution with thresholds that account for both the magnitude and the duration of exposure for the early and middle life stages whose survival governs the population. Two waters with the same winter minimum are therefore not equivalent, since exposure during reproduction, settlement or moulting does more damage than exposure at a tolerant stage, and a month below the threshold does more damage than a week.

The eastern Bering Sea shows that duration and season are not abstract concerns. Its shelf ranks among the most productive and corrosive seas because the decomposition of its large summer production, together with river runoff, removes carbonate from the bottom water [64]. A model hindcast for 1970 to 2022 finds that bottom water acidifies about twice as fast as surface water, that its pH has fallen to about 7.8, the level at which juvenile crabs begin to show symptoms in the laboratory, and that the shelf area with bottom water below that value grew from 5 to 10% before 2005 to more than half of the shelf by 2022 [65]. Surface water on the inner shelf is undersaturated for about half of the year [66, 67]. Juvenile red king crab (Paralithodes camtschaticus (Tilesius, 1815)) and Tanner crab

(Chionoecetes bairdi Rathbun, 1924) reared at reduced pH show lower survival and growth [68], and juvenile snow crabs (Chionoecetes opilio (Fabricius, 1788)) held at pH 7.5 suffer about 40% higher mortality than at present-day pH [69]. The Bering Sea snow crab population then collapsed, with the loss of more than ten billion animals between 2018 and 2021, mainly through a marine heatwave and starvation rather than acidification [45]. The collapse is nonetheless a clear case of a productive cold-water fishery pushed past a biological limit in a sea where acidification has reached levels shown to harm the same animals.

4.3 Calcifying plankton

Planktonic foraminifera provide supporting evidence from a comparison that spans more than a century. Comparing shells from an 1875 Challenger station with 2011 Tara Oceans material from the eastern equatorial Pacific, Fox et al. [38] found every modern specimen thinner, by up to 76% in *Neogloboquadrina dutertrei* and by up to about 30% in *Globigerinoides ruber*. The comparison is a single before-and-after pair, but foraminifera build low-magnesium calcite, one of the most acidification-resistant biominerals, so a signal of carbonate stress there suggests that even the hardiest plankton are affected.

Coccolithophores show why a single record must be read with care. Their occurrence in the North Atlantic rose roughly tenfold, from about 2% to over 20% of Continuous Plankton Recorder samples between 1965 and 2010, a rise tentatively linked to rising carbon dioxide [70]. Where calcification itself has been measured over decades, in the Gulf of Maine, it fell from about 0.4 to about 0.2 mg C per cubic metre per day between 2001 and

2018 [42, 43]. That decline, however, coincided with a change in the water entering the gulf, as warm and salty slope water displaced cooler and fresher water, and aragonite saturation rose over the seven years with carbonate data, so the record shows that calcification can fall steeply within decades without being evidence of acidification harming calcifiers. Tropical coccolithophore calcification has been found to be independent of carbonate chemistry [71], and some strains calcify more under high carbon dioxide [72].

4.4 Acidification in an already depleted ocean

Acidification is not arriving in an intact ocean, and the record of loss is long (Table 2). Some widely quoted figures are disputed, and we use the cautious ones. The often-quoted 90% loss of large predatory fish [37] is widely considered too high [73–75]. A few fast-declining populations can pull the Living Planet Index down [44], while others argue that many populations are still in real decline [76]. A synthesis of formal stock assessments places the decline in the adult biomass of tunas and their relatives at 52% over 1954 to 2006 [77]. Reported falls in Antarctic krill (Euphausia superba Dana, 1850) of 38 to 81% per decade in the southwest Atlantic sector [39] are challenged as partly a sampling artefact [41, 78], although a circumpolar reanalysis still finds a decline in the Atlantic sector [79] and a later analysis reports a southward contraction of the range [40]. None of these disputes changes the direction of travel, because biomass models, stock assessments, mammal counts and plankton records all show a clear decline in marine animal life.

Direct human pressure, rather than acidification, caused most of these losses through industrial fishing, whaling, bottom trawling, the destruction of coral reefs, oyster reefs and

mangroves, and widespread pollution. Climate disruption has added a growing share of the loss in recent decades, through ocean warming, marine heatwaves, coral bleaching and the loss of oxygen from the ocean [20, 80, 81]. Warming is the main driver of the halving of North Atlantic krill [35]. Coastal and estuarine systems carry the heaviest historical losses (Table 2) [46, 47]. Removing the largest fish also weakens the biological carbon pump, because the carbon held in their bodies and sinking waste no longer reaches the deep sea [82, 83]. Acidification is therefore acting on communities already thinned by other pressures, and that is the condition in which its effects must be judged.

The biocurve is offered in this context as an interpretive baseline rather than a census. Declining to synthesise is not a neutral choice, because it leaves no quantified baseline against which later change can be read, and that is how each generation comes to accept a depleted state as normal [84]. Our own field observations from a sailing passage of eighteen days across the tropical North Atlantic in the winter of 2022, which are anecdotal rather than systematic, are reported in Additional file 1, Note S4.

4.5 A hypothesised chemical cascade beyond the carbonate system

Aragonite saturation also tracks chemistry that sets the physical character of seawater, including its clarity and the ease with which a larva can move and feed. This section is a hypothesis, graded in the tiers of Section 2.9, and we set it out together with the observations that would confirm or refute the hypothesis. Two terms from colloid chemistry recur throughout the argument in this section. Zeta potential is the effective surface charge on particles, which decides whether they repel one another and stay

suspended or coagulate and settle, and redox potential is the net tendency of the water to oxidise or reduce.

In outline, the hypothesis runs as follows. The falling pH and carbonate ion concentration, together with the loss of buffer capacity [85], are expected to alter how organic matter coagulates and self-assembles into calcium-bridged gels, although that response has not yet been measured at open-ocean pH. A colloidal suspension then starts to develop, which provides the conditions in which bacterial numbers and turbidity increase. Bacterial respiration of that organic matter lowers the oxygen and the pH and reduces the buffer capacity further, and in our assessment the redox potential and the zeta potential fall with them. The result is a cascade of chemical reactions, a self-reinforcing loop that the carbonate buffer restrains or that stops when the bacteria run out of energy. The paragraphs below set out the established, the demonstrated and the hypothesised parts of that cascade in turn.

The established part of this argument is not in dispute in the chemical literature. Rising carbon dioxide lowers pH and carbonate ion concentration and consumes buffer capacity [85], and dissolved organic matter and inorganic colloids undergo pH-dependent charge neutralisation, coagulation and flocculation. As carbon dioxide diffuses through the surface microlayer, which can reduce gas transfer by up to about a third [86], pH falls, the zeta potential of suspended particles becomes less negative, and metal solubility rises, while total alkalinity is unchanged. Because marine particles already sit close to the coagulation threshold in high-ionic-strength seawater, even a modest shift in charge can have an effect.

643 The demonstrated part of the argument comes from engineered seawater systems and
644 aquaria. Ferric coagulation of organic matter and colloids is run at an industrial scale in
645 desalination pretreatment, where the high ionic strength of seawater compresses the
646 electrical double layer [87], and the coagulation of dissolved organic matter improves as
647 pH declines [88]. The formation of colloids as pH, redox potential and zeta potential
648 decrease, and its reversal as alkalinity, oxygen and redox potential are raised, are standard
649 and well-characterised processes in public aquaria and closed system aquaculture water
650 treatment. The novelty lies in applying that established chemistry to coastal and ocean
651 systems so that the net effect can be understood in the same terms. In operating records
652 from public aquaria holding 20 million litres, which the corresponding author kept in his
653 earlier work in water treatment and which are not published, these reactions accelerate
654 over about ten hours when buffering is lost, with measurable declines in water quality and
655 animal condition unless alkalinity, oxygen and redox potential are raised promptly. Aquaria
656 are enclosed and intensively managed, so they show that the chemistry is real, fast and
657 reversible, but they cannot show the rate or scale at which the same reactions would
658 proceed in open water.

659 The hypothesised part is that a falling pH raises the colloidal load and the micro-viscosity
660 of open-ocean water by an amount that matters for plankton. Micro-viscosity is the
661 effective viscosity experienced at the scale of small organisms and particles, which is set by
662 colloids and dissolved polymers rather than by the bulk water. Bacterial respiration of
663 organic matter lowers oxygen and pH together and consumes buffer capacity further [89],
664 acting on the calcium-bridged marine gels [90] described above. The final link of the chain
665 has been confirmed in the laboratory, where a modest rise in viscosity at constant

temperature slows the swimming and the feeding currents of planktonic larvae and small zooplankton [91, 92]. The link from falling pH to a higher colloidal load in the open ocean remains to be demonstrated directly (Section 3.5).

The hypothesis also has a consequence for plankton community structure. A more viscous and more colloidal surface layer is expected to favour small phytoplankton, such as cyanobacteria, most clearly in the warm subtropical gyres, and to slow microzooplankton and the larvae of larger animals more than large animals, because viscous forces dominate at small scales [91, 92]. Larger zooplankton and the larvae of fish and invertebrates must pass through that small stage, and cyanobacteria may be a poorer food for them, so less energy would reach the higher levels of the food web. We have not shown that this mechanism has caused any shift that has been observed, and the prediction should be tested alongside the measurements listed at the end of this section.

Iron is the element that links these chemical pathways most directly to productivity. It limits growth across the high-nutrient, low-chlorophyll regions that lie inside the low-saturation water [27], it is one of the most effective natural flocculants, and its chemical speciation is acutely sensitive to pH [93]. Acidification lowers the iron available to phytoplankton [94], while falling pH also speeds the reduction of ferric iron by dissolved polyphenols so that reduced iron persists for longer [95]. A recent review concludes that the net direction for iron, copper and zinc depends on which pH-controlled pathway dominates [96], and the response of the whole photochemical iron cycle of the sunlit layer [97, 98] still needs dedicated study.

Coastal dead zones show the end state of this sequence. The causality observed there runs from respiration and hypoxia to acidification, and the hypothesis adds that a loss of buffer would feed back on that process. The world has more than 500 such zones [80, 99], and where their carbonate chemistry has been measured, the hypoxic water is also acidified. Respiration of the eutrophication-driven organic load lowers the subsurface pH in the northern Gulf of Mexico and the East China Sea [89], and in Chesapeake Bay the bottom water reaches a pH of about 7.45 with aragonite saturation well below 1 [100]. Nutrient loading has crossed its own planetary boundary, at about three times the boundary for nitrogen and about twice the boundary for phosphorus [2]. The cascade also favours still water, and stratification has strengthened and ventilation weakened over the past half-century [101], while the oxygen content of the ocean has fallen [80, 81].

A dead zone develops by the same sequence. A trigger such as nutrient runoff, a marine heatwave or a spell of still, stratified water raises the organic load or lowers the supply of oxygen. On this hypothesis, the loss of buffer lets more matter coagulate, and the larger colloidal load feeds the bacteria that respire it, so the loop reinforces itself until the oxygen or the organic supply runs out. The risk is that a sequence that needs only a trigger to start spreads from enclosed coastal waters to larger areas as buffer capacity weakens, stratification strengthens and the ocean loses oxygen [80, 81, 101]. If it were initiated at scale, the biocurve could fall away earlier than the scenario in Figure 3, which remains a scenario and not a projection.

Satellite records offer a first and indirect test of the hypothesis. About 21% of the ocean darkened between 2003 and 2022, particularly in polar regions [102], and about 40% of

the ocean changed colour over two decades [103], but at productive sites the darkening cannot be separated from greening, because satellite attenuation and chlorophyll share the same blue-green band ratio. The Station ALOHA result (Section 3.5) is consistent with the hypothesis without confirming it, because a rise in biological supply is an equally plausible cause [21], and a rise in small cyanobacteria would darken the water in the same way, so counts of cyanobacteria there are the next test.

The hypothesis makes three testable predictions that existing programmes could check at modest cost. Adding redox potential, zeta potential, particle size and turbidity to the existing carbonate time-series stations would be inexpensive relative to the chemistry already collected there. A laboratory measurement of the coagulation response of natural seawater particles to a pH change of the size already recorded would test the central link directly. Over the coming decade, ocean-colour records can also test whether productivity in the high-nutrient, low-chlorophyll regions declines as saturation falls, which the hypothesis predicts but which has not yet been observed, since those regions have contracted at the poles since 2010 while chlorophyll there has risen [28].

4.6 Abrupt change and regional precedents

Three well-tested ideas explain why a sudden and lasting change of state is plausible in a thinned food web. Below a critical density, a strong Allee effect makes a population decline faster rather than more slowly [104, 105]. Diversity steadies fluctuating systems, so a food web that loses diversity also loses its buffer [106–108], even though complexity alone can destabilise a randomly assembled community [109]. Systems near a tipping point can shift

abruptly, sometimes with early-warning signals that are hard to read [110, 111]. None of this makes such a change certain, but it means that a stressed food web may not simply continue its present trend.

One regional end state is what Jackson [112] called the rise of slime, a simplified, microbially dominated system with blooms of toxic dinoflagellates and jellyfish, in which the large animals are greatly reduced. This end state has already appeared regionally in several ocean basins. Off Namibia, the Benguela sardine (Sardinops sagax (Jenyns, 1842)) stock collapsed under overfishing and was replaced by jellyfish and the bearded goby (Sufflogobius bibarbatus (von Bonde, 1923)), a state that has persisted for decades even after fishing was sharply reduced [113, 114, 115]. In the Black Sea, pollution, overfishing and an invading comb jelly (Mnemiopsis leidyi A. Agassiz, 1865) turned the open water to jelly in the 1980s [116, 117], with only partial recovery after pollution fell and a second invader reduced the comb jelly [118]. When Northwest Atlantic cod (Gadus morhua Linnaeus, 1758) collapsed in the early 1990s, forage fish, snow crab and shrimp took their place on the eastern Scotian Shelf [119], and like most collapsed fish stocks they showed little recovery within fifteen years [120, 121], and recovery becomes slower and less predictable the longer and deeper the depletion, so that at present harvest rates most depleted stocks are unlikely to recover [134]. Recovery is sometimes possible, since North Sea herring (Clupea harengus Linnaeus, 1758) rebuilt after the fishery was closed and carefully managed [121, 122].

These precedents are regional, and a worldwide rise of jellyfish is not supported, since the available synthesis shows roughly twenty-year oscillations rather than a steady global

increase [123, 124]. No mechanism is yet established by which regional shifts would propagate into a single global transition. A United Kingdom national security assessment published in 2026 nonetheless concludes, with high analytical confidence, that at current rates of biodiversity loss every critical ecosystem is on a pathway to collapse, while stating that it is not a scientific report and that its judgements on timing carry low confidence [125].

4.7 Limitations

Several limitations bound these results, and several of them would make the true exposure larger rather than smaller. The projections are linear extensions of 43-year trends, and they should be read as indicative beyond about 2045. The graded threshold is an ecological reference value rather than a lethal limit; only its two ends rest on measured responses, the values between them are interpolation, and the absolute share depends most on the warm-water end, which is why we quote the structural range and the sensitivity to that end rather than a single figure. A threshold defined by winter sea-surface temperature rather than latitude follows the same logic more closely; with the same two ends anchored at the zonal-mean winter temperatures of 10° and 60° (26.7 and 0.8 °C), it gives 38.2% now and 53.6% by 2045 (Additional file 1, Table S2), so the latitude ramp is the more conservative choice. The productivity weights are satellite proxies, not measurements of animal biomass, and they are annual means set against a winter saturation state, a mismatch that the month-by-month calculation of Section 3.3 addresses and that weakens the association. The projections leave out 2.5% of the mapped area that has no fitted trend (Section 2.4).

The analysis uses surface saturation, whereas many plankton spend the daylight hours in deeper and more corrosive water, and the sea-ice zone is not mapped, although adjacent polar water already lies below its threshold, so both omissions tend to understate exposure. Station K2 and Munida have too few winter casts for a fitted trend of their own. The biocurve is an interpretive synthesis of separately documented declines rather than a census, and its interpolated era values rest on a stated choice of curve. Finally, the chemical cascade of Section 4.5 remains a hypothesis.

5 Conclusions

The cold, productive waters that feed much of the marine food web are acidifying at rates that have persisted for four decades, and in winter they already sit at or below the threshold at which sensitive calcifiers respond. Judged at the winter minimum rather than the annual mean, about 35% of the mapped ocean surface, carrying 46% of the ocean's net primary production, the water that sustains the food web, is now below its ecological reference threshold.

This chemistry is acting on a marine system that fishing, whaling, habitat destruction, pollution and climate disruption had already depleted, with a loss of roughly 46 to 65% of its animal life since 1850 on our interpretive synthesis. Acidification did not cause those losses, but it now adds to them in communities with little capacity to spare, where the mechanisms of abrupt change are present vulnerabilities rather than distant possibilities.

Cutting carbon dioxide emissions and reducing harm will slow acidification but cannot reverse it, because the acidification of the ocean continues from past emissions and reversing it at the surface would need net removal of carbon dioxide [131], and groups that have lost about 70% of their numbers, such as marine mammals, sharks and seabirds (Table 2), may not recover without active restoration. In the decline scenario drawn in Figure 3, which continues the index at the 2023 slope of the interpolated curve, about 0.64 percentage points a year, a rate set by the assumed exponent of that curve, and then lets it accelerate, the importance-weighted loss would deepen from about 65% to about 78% by 2035; the shape of that scenario is a stated choice (Additional file 1, Note S3), so this is an illustration and not a prediction.

Ground minerals such as olivine, lime and calcium carbonate applied on land would raise the alkalinity of run-off and take up carbon dioxide as they weather, and so could raise the pH of the sea. Around 10 billion tonnes of olivine a year would be needed to match the anthropogenic carbon dioxide that the ocean now takes up each year [130, 135], about the same mass as the coal mined in the world each year, some 9 billion tonnes [132], and a following report examines how this could be done.

We draw four practical conclusions for monitoring, reporting and management from this study. First, ocean acidification should be treated as an active component of cumulative marine risk now, not solely as a future concern. Second, saturation should be reported at the winter minimum and with the duration of the corrosive season, alongside annual means, because biological thresholds are defined by exposure. Third, redox potential, zeta potential and particle measurements should be added to existing carbonate time-series

stations so that the hypothesised chemical cascade can be tested rather than argued. Fourth, because reversal becomes a matter of regeneration as critical densities are crossed, the protection and restoration of productive cold-water and coastal systems should begin now while recovery remains possible.

It is no longer sufficient to do no harm; it is time to do some good, to actively restore damaged ecosystems and to regenerate nature in all its forms, while there may still be time.

Abbreviations

CCI: Climate Change Initiative
CODAP-NA: Coastal Ocean Data Analysis Product in North America
ERDDAP: Environmental Research Division's Data Access Program
ESA: European Space Agency
GLODAP: Global Ocean Data Analysis Project
JAMSTEC: Japan Agency for Marine-Earth Science and Technology
Kd490: diffuse attenuation coefficient at 490 nm
MODIS: Moderate Resolution Imaging Spectroradiometer
NCEI: National Centers for Environmental Information
NOAA: National Oceanic and Atmospheric Administration
OCADS: Ocean Carbon and Acidification Data System
pCO_2: partial pressure of carbon dioxide
SPOTS: Synthesis Product for Ocean Time Series
Ω: aragonite saturation state

Declarations

Ethics approval and consent to participate

Not applicable, because the study used only published and publicly archived data.

Consent for publication

Not applicable, because the manuscript contains no data from any individual person.

Availability of data and materials

The datasets supporting the conclusions of this article are available in the NOAA National Centers for Environmental Information repository, OceanSODA-ETHZ v2025, accession 0220059, https://doi.org/10.25921/m5wx-ja34, and in the Zenodo repository, https://doi.org/10.5281/zenodo.21970808. The MODIS-Aqua products used for the productivity weighting are available from NOAA CoastWatch ERDDAP (datasets erdMH1ppmday, erdMPICmday and erdMH1chlamday, accessed 9 October 2026). The Zenodo deposit holds the recomputed cast-level saturation values, the winter threshold grids, the uncertainty ensembles and all analysis and figure code under a CC BY 4.0 licence, together with the block-mean productivity weights, the graded-threshold grids and the weighting scripts added for this revision. Every other primary dataset used in this study is public and is listed in Table 1 with its accession or citation.

Competing interests

The authors declare that they have no conflict of interest. Both authors are affiliated with the GOES Foundation, a non-profit marine science and conservation organisation. Howard Dryden founded Dryden Aqua Ltd and is the inventor of AFM-activated filter media; he left the company in 2020 and has since sold his entire shareholding, so he holds no financial interest in the company. That background in water treatment is the source of the colloid and coagulation chemistry applied in this study.

Funding

The GOES Foundation supported this research, which received no external grant funding.

Authors' contributions

Howard Dryden and Diane Duncan jointly conceived and designed the study reported here. Howard Dryden compiled and analysed the data, computed the saturation values, built the figures and the biocurve, and drafted the manuscript. Diane Duncan contributed the biological interpretation and revised the manuscript, and both authors approved the final version.

Acknowledgements

The authors thank the investigators, programmes and data centres whose sustained observations made this study possible, including the SPOTS time-series synthesis, the Iceland Sea time series of Jón Ólafsson and colleagues, the Irminger Sea programme, Station K2 (JAMSTEC), the Munida time series, the OceanSODA-ETHZ product of Luke Gregor and Nicolas Gruber, the Continuous Plankton Recorder survey, the MODIS Ocean Biology Processing Group and NOAA CoastWatch.

References

1. National Research Council. Ocean acidification: a national strategy to meet the challenges of a changing ocean. Washington, DC: The National Academies Press; 2010. https://doi.org/10.17226/12904

2. Richardson K, et al. Earth beyond six of nine planetary boundaries. Science Advances. 2023;9:eadh2458. https://doi.org/10.1126/sciadv.adh2458

3. Rockström J, et al. A safe operating space for humanity. Nature. 2009;461:472–475. https://doi.org/10.1038/461472a

4. Findlay HS, et al. Ocean Acidification: Another Planetary Boundary Crossed. Global Change Biology. 2025;31:e70238. https://doi.org/10.1111/gcb.70238

5. Gregor L, Gruber N. OceanSODA-ETHZ: a global gridded data set of the surface ocean carbonate system for seasonal to decadal studies of ocean acidification. Earth System Science Data. 2021;13:777–808. https://doi.org/10.5194/essd-13-777-2021

6. Gregor L, Gruber N. OceanSODA-ETHZ: a global gridded dataset of the surface ocean carbonate system for seasonal to decadal studies of ocean acidification (v2025) (NCEI Accession 0220059) [dataset]. Subset used: omega_ar and omega_ar_uncert, 1982–2024. NOAA National Centers for Environmental Information; 2020. https://doi.org/10.25921/m5wx-ja34. Accessed 23 Aug 2026.

7. Lange N, et al. Synthesis Product for Ocean Time Series (SPOTS) – a ship-based biogeochemical pilot. Earth System Science Data. 2024;16:1901–1931. https://doi.org/10.5194/essd-16-1901-2024

8. Lauvset SK, et al. GLODAPv2.2022: the latest version of the global interior ocean biogeochemical data product. Earth System Science Data. 2022;14:5543–5572. https://doi.org/10.5194/essd-14-5543-2022

9. Jiang LQ, et al. Coastal Ocean Data Analysis Product in North America (CODAP-NA) – an internally consistent data product for discrete inorganic carbon, oxygen, and nutrients on the North American ocean margins. Earth System Science Data. 2021;13:2777–2799. https://doi.org/10.5194/essd-13-2777-2021

10. Humphreys MP, Lewis ER, Sharp JD, Pierrot D. PyCO2SYS v1.8: marine carbonate system calculations in Python. Geoscientific Model Development. 2022;15:15–43. https://doi.org/10.5194/gmd-15-15-2022

11. Lueker TJ, Dickson AG, Keeling CD. Ocean pCO_2 calculated from dissolved inorganic carbon, alkalinity, and equations for K_1 and K_2: validation based on laboratory measurements of CO_2 in gas and seawater at equilibrium. Marine Chemistry. 2000;70:105–119. https://doi.org/10.1016/S0304-4203(00)00022-0

12. Dickson AG. Standard potential of the reaction: AgCl(s) + 0.5H2(g) = Ag(s) + HCl(aq), and the standard acidity constant of the ion HSO4- in synthetic sea water from 273.15 to 318.15 K. Journal of Chemical Thermodynamics. 1990;22:113–127. https://doi.org/10.1016/0021-9614(90)90074-Z

13. Uppström LR. The boron/chlorinity ratio of deep-sea water from the Pacific Ocean. Deep-Sea Research and Oceanographic Abstracts. 1974;21:161–162. https://doi.org/10.1016/0011-7471(74)90074-6

14. Orr JC, Epitalon JM, Dickson AG, Gattuso JP. Routine uncertainty propagation for the marine carbon dioxide system. Marine Chemistry. 2018;207:84–107. https://doi.org/10.1016/j.marchem.2018.10.006

15. Sulpis O, Lauvset SK, Hagens M. Current estimates of K_1* and K_2* appear inconsistent with measured CO_2 system parameters in cold oceanic regions. Ocean Science. 2020;16:847–862. https://doi.org/10.5194/os-16-847-2020

16. Ólafsson J, Ólafsdóttir SR, Benoit-Cattin A, Takahashi T. The Irminger Sea and the Iceland Sea time series measurements of sea water carbon and nutrient chemistry 1983–2008. Earth System Science Data. 2010;2:99–104. https://doi.org/10.5194/essd-2-99-2010

17. Waldbusser GG, et al. Saturation-state sensitivity of marine bivalve larvae to ocean acidification. Nature Climate Change. 2015;5:273–280. https://doi.org/10.1038/nclimate2479

18. Hofmann Elizondo U, et al. The impact of aragonite saturation variability on shelled pteropods: an attribution study in the California Current System. Global Change Biology. 2024;30:e17345. https://doi.org/10.1111/gcb.17345

19. Bednaršek N, Feely RA, Pelletier G, Desmet F. Global synthesis of the status and trends of ocean acidification impacts on shelled pteropods. Oceanography. 2023;36:130–137. https://doi.org/10.5670/oceanog.2023.210

20. Hoegh-Guldberg O, et al. Coral reefs under rapid climate change and ocean acidification. Science. 2007;318:1737–1742. https://doi.org/10.1126/science.1152509

21. Kavanaugh MT, et al. ALOHA From the Edge: Reconciling Three Decades of in Situ Eulerian Observations and Geographic Variability in the North Pacific Subtropical Gyre. Frontiers in Marine Science. 2018;5:130. https://doi.org/10.3389/fmars.2018.00130

22. Ólafsson J, et al. Rate of Iceland Sea acidification from time-series measurements. Biogeosciences. 2009;6:2661–2668. https://doi.org/10.5194/bg-6-2661-2009

23. OSPAR Commission. Ocean acidification thematic assessment. OSPAR Quality Status Report 2023. London: OSPAR Commission; 2023. https://oap.ospar.org/en/ospar-assessments/quality-status-reports/qsr-2023/other-assessments/ocean-acidification/. Accessed 23 Sep 2026.

24. Honda MC, et al. Comparison of carbon cycle between the western Pacific subarctic and subtropical time-series stations: highlights of the K2S1 project. Journal of Oceanography. 2017;73:647–667. https://doi.org/10.1007/s10872-017-0423-3

25. Vance JM, Currie KC, Suanda SH, Law CS. Drivers of seasonal to decadal mixed layer carbon cycle variability in subantarctic water in the Munida Time Series. Frontiers in Marine Science. 2024;11:1309560. https://doi.org/10.3389/fmars.2024.1309560

26. Ma D, Gregor L, Gruber N. Four decades of trends and drivers of global surface ocean acidification. Global Biogeochemical Cycles. 2023;37:e2023GB007765. https://doi.org/10.1029/2023GB007765

27. Martin JH, Fitzwater SE. Iron deficiency limits phytoplankton growth in the north-east Pacific subarctic. Nature. 1988;331:341–343. https://doi.org/10.1038/331341a0

28. Basterretxea G, Font-Muñoz JS, Hernández-Carrasco I, Sañudo-Wilhelmy SA. Global variability of high-nutrient low-chlorophyll regions using neural networks and wavelet coherence analysis. Ocean Science. 2023;19:973–990. https://doi.org/10.5194/os-19-973-2023

29. Greenspoon L, et al. The global biomass of mammals since 1850. Nature Communications. 2025;16:8338. https://doi.org/10.1038/s41467-025-63888-z

30. Bianchi D, et al. Estimating global biomass and biogeochemical cycling of marine fish with and without fishing. Science Advances. 2021;7:eabd7554. https://doi.org/10.1126/sciadv.abd7554

31. Christensen V, Coll M, Piroddi C, Steenbeek J, Buszowski J, Pauly D. A century of fish biomass decline in the ocean. Marine Ecology Progress Series. 2014;512:155–166. https://doi.org/10.3354/meps10946

32. Pacoureau N, et al. Half a century of global decline in oceanic sharks and rays. Nature. 2021;589:567–571. https://doi.org/10.1038/s41586-020-03173-9

33. Paleczny M, Hammill E, Karpouzi V, Pauly D. Population trend of the world's monitored seabirds, 1950-2010. PLOS ONE. 2015;10:e0129342. https://doi.org/10.1371/journal.pone.0129342

34. Eddy TD, et al. Global decline in capacity of coral reefs to provide ecosystem services. One Earth. 2021;4:1278–1285. https://doi.org/10.1016/j.oneear.2021.08.016

35. Edwards M, et al. North Atlantic warming over six decades drives decreases in krill abundance with no associated range shift. Communications Biology. 2021;4:644. https://doi.org/10.1038/s42003-021-02159-1

36. WWF. Living Planet Report 2024: a system in peril. Gland: WWF; 2024.

37. Myers RA, Worm B. Rapid worldwide depletion of predatory fish communities. Nature. 2003;423:280–283. https://doi.org/10.1038/nature01610

38. Fox L, Stukins S, Hill T, Miller CG. Quantifying the effect of anthropogenic climate change on calcifying plankton. Scientific Reports. 2020;10:1620. https://doi.org/10.1038/s41598-020-58501-w

39. Atkinson A, Siegel V, Pakhomov E, Rothery P. Long-term decline in krill stock and increase in salps within the Southern Ocean. Nature. 2004;432:100–103. https://doi.org/10.1038/nature02996

40. Atkinson A, et al. Krill (*Euphausia superba*) distribution contracts southward during rapid regional warming. Nature Climate Change. 2019;9:142–147. https://doi.org/10.1038/s41558-018-0370-z

41. Cox MJ, et al. No evidence for a decline in the density of Antarctic krill Euphausia superba Dana, 1850, in the Southwest Atlantic sector between 1976 and 2016. Journal of Crustacean Biology. 2018;38:656–661. https://doi.org/10.1093/jcbiol/ruy072

42. Balch WM, et al. Changing hydrographic, biogeochemical, and acidification properties in the Gulf of Maine as measured by the Gulf of Maine North Atlantic Time Series, GNATS, between 1998 and 2018. Journal of Geophysical Research: Biogeosciences. 2022;127:e2022JG006790. https://doi.org/10.1029/2022JG006790

43. Marsh NLJ, et al. Updated global compilation of coccolithophore calcification measurements from unperturbed water samples including ancillary data [dataset]. PANGAEA; 2025. https://doi.org/10.1594/PANGAEA.987673

44. Leung B, et al. Clustered versus catastrophic global vertebrate declines. Nature. 2020;588:267–271. https://doi.org/10.1038/s41586-020-2920-6

45. Szuwalski CS, Aydin K, Fedewa EJ, Garber-Yonts B, Litzow MA. The collapse of eastern Bering Sea snow crab. Science. 2023;382:306–310. https://doi.org/10.1126/science.adf6035

46. Beck MW, et al. Oyster reefs at risk and recommendations for conservation, restoration, and management. BioScience. 2011;61:107–116. https://doi.org/10.1525/bio.2011.61.2.5

47. Lotze HK, Lenihan HS, Bourque BJ, Bradbury RH, Cooke RG, Kay MC, et al. Depletion, degradation, and recovery potential of estuaries and coastal seas. Science. 2006;312:1806–1809. https://doi.org/10.1126/science.1128035

48. Jiang LQ, et al. Climatological distribution of aragonite saturation state in the global oceans. Global Biogeochemical Cycles. 2015;29:1656–1673. https://doi.org/10.1002/2015GB005198

49. Negrete-García G, et al. Sudden emergence of a shallow aragonite saturation horizon in the Southern Ocean. Nature Climate Change. 2019;9:313–317. https://doi.org/10.1038/s41558-019-0418-8

50. Orr JC, et al. Anthropogenic ocean acidification over the twenty-first century and its impact on calcifying organisms. Nature. 2005;437:681–686. https://doi.org/10.1038/nature04095

51. Bednaršek N, et al. *Limacina helicina* shell dissolution as an indicator of declining habitat suitability owing to ocean acidification in the California Current Ecosystem. Proceedings of the Royal Society B. 2014;281:20140123. https://doi.org/10.1098/rspb.2014.0123

52. Bednaršek N, et al. Extensive dissolution of live pteropods in the Southern Ocean. Nature Geoscience. 2012;5:881–885. https://doi.org/10.1038/ngeo1635

53. Caesar L, Rahmstorf S, Robinson A, Feulner G, Saba V. Observed fingerprint of a weakening Atlantic Ocean overturning circulation. Nature. 2018;556:191–196. https://doi.org/10.1038/s41586-018-0006-5

54. Curbelo-Hernández D, Pérez FF, González-Dávila M, Gladyshev SV, González AG, González-Santana D, et al. Ocean acidification trends and carbonate system dynamics across the North Atlantic subpolar gyre water masses during 2009–2019. Biogeosciences. 2024;21:5561–5589. https://doi.org/10.5194/bg-21-5561-2024

55. Kleypas JA, et al. Geochemical consequences of increased atmospheric carbon dioxide on coral reefs. Science. 1999;284:118–120. https://doi.org/10.1126/science.284.5411.118

56. Barton A, et al. Impacts of coastal acidification on the Pacific Northwest shellfish industry and adaptation strategies implemented in response. Oceanography. 2015;28(2):146–159. https://doi.org/10.5670/oceanog.2015.38

57. Lebrato M, et al. Benthic marine calcifiers coexist with $CaCO_3$-undersaturated seawater worldwide. Global Biogeochemical Cycles. 2016;30:1038–1053. https://doi.org/10.1002/2015GB005260

58. Cyronak T, Schulz KG, Jokiel PL. The Omega myth: what really drives lower calcification rates in an acidifying ocean. ICES J Mar Sci. 2016;73:558–562. https://doi.org/10.1093/icesjms/fsv075

59. Hardie LA. Secular variation in seawater chemistry: an explanation for the coupled secular variation in the mineralogies of marine limestones and potash evaporites over the past 600 m.y. Geology. 1996;24:279–283. https://doi.org/10.1130/0091-7613(1996)024<0279:SVISCA>2.3.CO;2

60. Stanley SM, Hardie LA. Secular oscillations in the carbonate mineralogy of reef-building and sediment-producing organisms driven by tectonically forced shifts in seawater chemistry. Palaeogeography, Palaeoclimatology, Palaeoecology. 1998;144:3–19. https://doi.org/10.1016/S0031-0182(98)00109-6

61. Ries JB. Review: geological and experimental evidence for secular variation in seawater Mg/Ca (calcite-aragonite seas) and its effects on marine biological calcification. Biogeosciences. 2010;7:2795–2849. https://doi.org/10.5194/bg-7-2795-2010

62. Andersson AJ, Mackenzie FT, Bates NR. Life on the margin: implications of ocean acidification on Mg-calcite, high-latitude and cold-water marine calcifiers. Marine Ecology Progress Series. 2008;373:265–273. https://doi.org/10.3354/meps07639

63. Ries JB, Cohen AL, McCorkle DC. Marine calcifiers exhibit mixed responses to CO_2-induced ocean acidification. Geology. 2009;37:1131–1134. https://doi.org/10.1130/G30210A.1

64. Mathis JT, Cross JN, Bates NR. Coupling primary production and terrestrial runoff to ocean acidification and carbonate mineral suppression in the eastern Bering Sea. Journal of Geophysical Research: Oceans. 2011;116:C02030. https://doi.org/10.1029/2010JC006453

65. Pilcher DJ, Cross JN, Monacci N, Mu L, Kearney KA, Hermann AJ, et al. Amplified bottom water acidification rates on the Bering Sea shelf from 1970–2022. Biogeosciences. 2025;22:3103–3125. https://doi.org/10.5194/bg-22-3103-2025

66. Mathis JT, Cross JN, Monacci N, Feely RA, Stabeno P. Evidence of prolonged aragonite undersaturations in the bottom waters of the southern Bering Sea shelf from autonomous sensors. Deep-Sea Research Part II. 2014;109:125–133. https://doi.org/10.1016/j.dsr2.2013.07.019

67. Pilcher DJ, Naiman DM, Cross JN, Hermann AJ, Siedlecki SA, Gibson GA, et al. Modeled effect of coastal biogeochemical processes, climate variability, and ocean acidification on aragonite saturation state in the Bering Sea. Frontiers in Marine Science. 2019;5:508. https://doi.org/10.3389/fmars.2018.00508

68. Long WC, Swiney KM, Harris C, Page HN, Foy RJ. Effects of ocean acidification on juvenile red king crab (Paralithodes camtschaticus) and Tanner crab (Chionoecetes bairdi) growth, condition, calcification, and survival. PLOS ONE. 2013;8:e60959. https://doi.org/10.1371/journal.pone.0060959

69. Long WC. Ocean acidification reduces juvenile snow crab, Chionoecetes opilio, survival but does not affect growth or morphometrics. Journal of Experimental Marine Biology and Ecology. 2026;594:152153. https://doi.org/10.1016/j.jembe.2025.152153

70. Rivero-Calle S, et al. Multidecadal increase in North Atlantic coccolithophores and the potential role of rising CO_2. Science. 2015;350:1533–1537. https://doi.org/10.1126/science.aaa8026

71. Marañón E, et al. Coccolithophore calcification is independent of carbonate chemistry in the tropical ocean. Limnology and Oceanography. 2016;61:1345–1357. https://doi.org/10.1002/lno.10295

72. Iglesias-Rodriguez MD, et al. Phytoplankton calcification in a high-CO_2 world. Science. 2008;320:336–340. https://doi.org/10.1126/science.1154122

73. Hampton J, et al. Decline of Pacific tuna populations exaggerated? Nature. 2005;434:E1–E2. https://doi.org/10.1038/nature03581

74. Polacheck T. Tuna longline catch rates in the Indian Ocean: did industrial fishing result in a 90% rapid decline in the abundance of large predatory species? Marine Policy. 2006;30:470–482. https://doi.org/10.1016/j.marpol.2005.06.016

75. Sibert J, et al. Biomass, size, and trophic status of top predators in the Pacific Ocean. Science. 2006;314:1773–1776. https://doi.org/10.1126/science.1135347

76. Loreau M, et al. Do not downplay biodiversity loss. Nature. 2022;601:E27–E28. https://doi.org/10.1038/s41586-021-04179-7

77. Juan-Jordá MJ, Mosqueira I, Cooper AB, Freire J, Dulvy NK. Global population trajectories of tunas and their relatives. Proceedings of the National Academy of Sciences USA. 2011;108:20650–20655. https://doi.org/10.1073/pnas.1107743108

78. Hill SL, et al. Observing change in pelagic animals as sampling methods shift: the case of Antarctic krill. Frontiers in Marine Science. 2024;11:1307402. https://doi.org/10.3389/fmars.2024.1307402

79. Yang G, et al. Changing circumpolar distributions and isoscapes of Antarctic krill: Indo-Pacific habitat refuges counter long-term degradation of the Atlantic sector. Limnology and Oceanography. 2021;66:272–287. https://doi.org/10.1002/lno.11603

80. Breitburg D, et al. Declining oxygen in the global ocean and coastal waters. Science. 2018;359:eaam7240. https://doi.org/10.1126/science.aam7240

81. Schmidtko S, Stramma L, Visbeck M. Decline in global oceanic oxygen content during the past five decades. Nature. 2017;542:335–339. https://doi.org/10.1038/nature21399

82. Mariani G, et al. Let more big fish sink: fisheries prevent blue carbon sequestration – half in unprofitable areas. Science Advances. 2020;6:eabb4848. https://doi.org/10.1126/sciadv.abb4848

83. Saba GK, et al. Toward a better understanding of fish-based contribution to ocean carbon flux. Limnology and Oceanography. 2021;66:1639–1664. https://doi.org/10.1002/lno.11709

84. Pauly D. Anecdotes and the shifting baseline syndrome of fisheries. Trends in Ecology and Evolution. 1995;10:430. https://doi.org/10.1016/S0169-5347(00)89171-5

85. Egleston ES, Sabine CL, Morel FMM. Revelle revisited: buffer factors that quantify the response of ocean chemistry to changes in DIC and alkalinity. Global Biogeochemical Cycles. 2010;24:GB1002. https://doi.org/10.1029/2008GB003407

86. Pereira R, Ashton I, Sabbaghzadeh B, Shutler JD, Upstill-Goddard RC. Reduced air–sea CO_2 exchange in the Atlantic Ocean due to biological surfactants. Nature Geoscience. 2018;11:492–496. https://doi.org/10.1038/s41561-018-0136-2

87. Edzwald JK, Haarhoff J. Seawater pretreatment for reverse osmosis: chemistry, contaminants, and coagulation. Water Research. 2011;45:5428–5440. https://doi.org/10.1016/j.watres.2011.08.014

88. Duan J, Gregory J. Coagulation by hydrolysing metal salts. Advances in Colloid and Interface Science. 2003;100–102:475–502. https://doi.org/10.1016/S0001-8686(02)00067-2

89. Cai WJ, et al. Acidification of subsurface coastal waters enhanced by eutrophication. Nature Geoscience. 2011;4:766–770. https://doi.org/10.1038/ngeo1297

90. Verdugo P. Marine microgels. Annual Review of Marine Science. 2012;4:375–400. https://doi.org/10.1146/annurev-marine-120709-142759

91. Podolsky RD, Emlet RB. Separating the effects of temperature and viscosity on swimming and water movement by sand dollar larvae (Dendraster excentricus). Journal of Experimental Biology. 1993;176:207–222. https://doi.org/10.1242/jeb.176.1.207

92. Larsen PS, Madsen CV, Riisgård HU. Effect of temperature and viscosity on swimming velocity of the copepod Acartia tonsa, brine shrimp Artemia salina and rotifer Brachionus plicatilis. Aquatic Biology. 2008;4:47–54. https://doi.org/10.3354/ab00093

93. Millero FJ, Woosley R, DiTrolio B, Waters J. Effect of ocean acidification on the speciation of metals in seawater. Oceanography. 2009;22:72–85. https://doi.org/10.5670/oceanog.2009.98

94. Shi D, Xu Y, Hopkinson BM, Morel FMM. Effect of ocean acidification on iron availability to marine phytoplankton. Science. 2010;327:676–679. https://doi.org/10.1126/science.1183517

95. Pérez-Almeida N, González AG, Santana-Casiano JM, González-Dávila M. Ocean acidification effect on the iron-gallic acid redox interaction in seawater. Frontiers in Marine Science. 2022;9:837363. https://doi.org/10.3389/fmars.2022.837363

96. Cheriyan E, Kumar BSK, Gupta GVM, Rao DB. Implications of ocean acidification on micronutrient elements, iron, copper and zinc, and their primary biological impacts: a review. Marine Pollution Bulletin. 2024;199:115991. https://doi.org/10.1016/j.marpolbul.2023.115991

97. Barbeau K, Rue EL, Bruland KW, Butler A. Photochemical cycling of iron in the surface ocean mediated by microbial iron(III)-binding ligands. Nature. 2001;413:409–413. https://doi.org/10.1038/35096545

98. Voelker BM, Morel FMM, Sulzberger B. Iron redox cycling in surface waters: effects of humic substances and light. Environmental Science and Technology. 1997;31:1004–1011. https://doi.org/10.1021/es9604018

99. Diaz RJ, Rosenberg R. Spreading dead zones and consequences for marine ecosystems. Science. 2008;321:926–929. https://doi.org/10.1126/science.1156401

100. Cai WJ, et al. Redox reactions and weak buffering capacity lead to acidification in the Chesapeake Bay. Nature Communications. 2017;8:369. https://doi.org/10.1038/s41467-017-00417-7

101. Li G, Cheng L, Zhu J, Trenberth KE, Mann ME, Abraham JP. Increasing ocean stratification over the past half-century. Nature Climate Change. 2020;10:1116–1123. https://doi.org/10.1038/s41558-020-00918-2

102. Davies TW, Smyth T. Darkening of the global ocean. Global Change Biology. 2025;31:e70227. https://doi.org/10.1111/gcb.70227

103. Cael BB, Bisson K, Boss E, Dutkiewicz S, Henson S. Global climate-change trends detected in indicators of ocean ecology. Nature. 2023;619:551–554. https://doi.org/10.1038/s41586-023-06321-z

104. Courchamp F, Berec L, Gascoigne J. Allee effects in ecology and conservation. Oxford: Oxford University Press; 2008. https://doi.org/10.1093/acprof:oso/9780198570301.001.0001

105. Stephens PA, Sutherland WJ. Consequences of the Allee effect for behaviour, ecology and conservation. Trends in Ecology and Evolution. 1999;14:401–405. https://doi.org/10.1016/S0169-5347(99)01684-5

106. Loreau M, de Mazancourt C. Biodiversity and ecosystem stability: a synthesis of underlying mechanisms. Ecology Letters. 2013;16:106–115. https://doi.org/10.1111/ele.12073

107. Tilman D, Lehman CL, Bristow CE. Diversity–stability relationships: statistical inevitability or ecological consequence? American Naturalist. 1998;151:277–282. https://doi.org/10.1086/286118

108. Yachi S, Loreau M. Biodiversity and ecosystem productivity in a fluctuating environment: the insurance hypothesis. Proc Natl Acad Sci USA. 1999;96:1463–1468. https://doi.org/10.1073/pnas.96.4.1463

109. May RM. Will a large complex system be stable? Nature. 1972;238:413–414. https://doi.org/10.1038/238413a0

110. Scheffer M, et al. Early-warning signals for critical transitions. Nature. 2009;461:53–59. https://doi.org/10.1038/nature08227

111. Boettiger C, Hastings A. Quantifying limits to detection of early warning for critical transitions. J R Soc Interface. 2012;9:2527–2539. https://doi.org/10.1098/rsif.2012.0125

112. Jackson JBC. Ecological extinction and evolution in the brave new ocean. Proc Natl Acad Sci USA. 2008;105 Suppl 1:11458–11465. https://doi.org/10.1073/pnas.0802812105

113. Utne-Palm AC, et al. Trophic structure and community stability in an overfished ecosystem. Science. 2010;329:333–336. https://doi.org/10.1126/science.1190708

114. Lynam CP, et al. Jellyfish overtake fish in a heavily fished ecosystem. Current Biology. 2006;16:R492–R493. https://doi.org/10.1016/j.cub.2006.06.018

115. Roux JP, van der Lingen CD, Gibbons MJ, Moroff NE, Shannon LJ, Smith ADM, et al. Jellyfication of marine ecosystems as a likely consequence of overfishing small pelagic fishes: lessons from the Benguela. Bulletin of Marine Science. 2013;89:249–284. https://doi.org/10.5343/bms.2011.1145

116. Daskalov GM, Grishin AN, Rodionov S, Mihneva V. Trophic cascades triggered by overfishing reveal possible mechanisms of ecosystem regime shifts. Proc Natl Acad Sci USA. 2007;104:10518–10523. https://doi.org/10.1073/pnas.0701100104

117. Oguz T, Fach B, Salihoglu B. Invasion dynamics of the alien ctenophore *Mnemiopsis leidyi* and its impact on anchovy collapse in the Black Sea. Journal of Plankton Research. 2008;30:1385–1397. https://doi.org/10.1093/plankt/fbn094

118. Kideys AE. Fall and rise of the Black Sea ecosystem. Science. 2002;297:1482–1484. https://doi.org/10.1126/science.1073002

119. Frank KT, Petrie B, Choi JS, Leggett WC. Trophic cascades in a formerly cod-dominated ecosystem. Science. 2005;308:1621–1623. https://doi.org/10.1126/science.1113075

120. Hutchings JA, Reynolds JD. Marine fish population collapses: consequences for recovery and extinction risk. BioScience. 2004;54:297–309. https://doi.org/10.1641/0006-3568(2004)054[0297:MFPCCF]2.0.CO;2

121. Lotze HK, Coll M, Magera AM, Ward-Paige C, Airoldi L. Recovery of marine animal populations and ecosystems. Trends in Ecology and Evolution. 2011;26:595–605. https://doi.org/10.1016/j.tree.2011.07.008

122. Dickey-Collas M, et al. Lessons learned from stock collapse and recovery of North Sea herring: a review. ICES Journal of Marine Science. 2010;67:1875–1886. https://doi.org/10.1093/icesjms/fsq033

123. Condon RH, et al. Questioning the rise of gelatinous zooplankton in the world's oceans. BioScience. 2012;62:160–169. https://doi.org/10.1525/bio.2012.62.2.9

124. Condon RH, et al. Recurrent jellyfish blooms are a consequence of global oscillations. Proc Natl Acad Sci USA. 2013;110:1000–1005. https://doi.org/10.1073/pnas.1210920110

125. HM Government. Nature security assessment on global biodiversity loss, ecosystem collapse and national security. London: Department for Environment, Food and Rural Affairs; 2026. https://www.gov.uk/government/publications/nature-security-assessment-on-global-biodiversity-loss-ecosystem-collapse-and-national-security. Accessed 23 Sep 2026.

126. Behrenfeld MJ, Falkowski PG. Photosynthetic rates derived from satellite-based chlorophyll concentration. Limnology and Oceanography. 1997;42:1–20. https://doi.org/10.4319/lo.1997.42.1.0001

127. Balch WM, Gordon HR, Bowler BC, Drapeau DT, Booth ES. Calcium carbonate measurements in the surface global ocean based on Moderate-Resolution Imaging Spectroradiometer data. Journal of Geophysical Research. 2005;110:C07001. https://doi.org/10.1029/2004JC002560

128. Hönisch B, Ridgwell A, Schmidt DN, Thomas E, Gibbs SJ, Sluijs A, et al. The geological record of ocean acidification. Science. 2012;335:1058–1063. https://doi.org/10.1126/science.1208277

129. Scotese CR, Song H, Mills BJW, van der Meer DG. Phanerozoic paleotemperatures: the earth's changing climate during the last 540 million years. Earth-Science Reviews. 2021;215:103503. https://doi.org/10.1016/j.earscirev.2021.103503

130. Friedlingstein P, O'Sullivan M, Jones MW, Andrew RM, Hauck J, Landschützer P, et al. Global Carbon Budget 2024. Earth System Science Data. 2025;17:965–1039. https://doi.org/10.5194/essd-17-965-2025

131. IPCC. Climate Change 2021: the physical science basis. Contribution of Working Group I to the Sixth Assessment Report of the Intergovernmental Panel on Climate Change. Cambridge: Cambridge University Press; 2023. https://doi.org/10.1017/9781009157896

132. International Energy Agency. Coal 2024: analysis and forecast to 2027. Paris: IEA; 2024. https://www.iea.org/reports/coal-2024

133. Ministry of Fisheries. Harvest Strategy Standard for New Zealand Fisheries. Wellington: Ministry of Fisheries; 2008. https://fs.fish.govt.nz/Doc/16543/harveststrategyfinal.pdf.ashx

134. Neubauer P, Jensen OP, Hutchings JA, Baum JK. Resilience and recovery of overexploited marine populations. Science. 2013;340:347–349. https://doi.org/10.1126/science.1230441

135. Hartmann J, West AJ, Renforth P, Köhler P, De La Rocha CL, Wolf-Gladrow DA, et al. Enhanced chemical weathering as a geoengineering strategy to reduce atmospheric carbon dioxide, supply nutrients, and mitigate ocean acidification. Reviews of Geophysics. 2013;51:113–149. https://doi.org/10.1002/rog.20004

136. Plaisance L, Caley MJ, Brainard RE, Knowlton N. The diversity of coral reefs: what are we missing? PLoS ONE. 2011;6:e25026. https://doi.org/10.1371/journal.pone.0025026

Figures

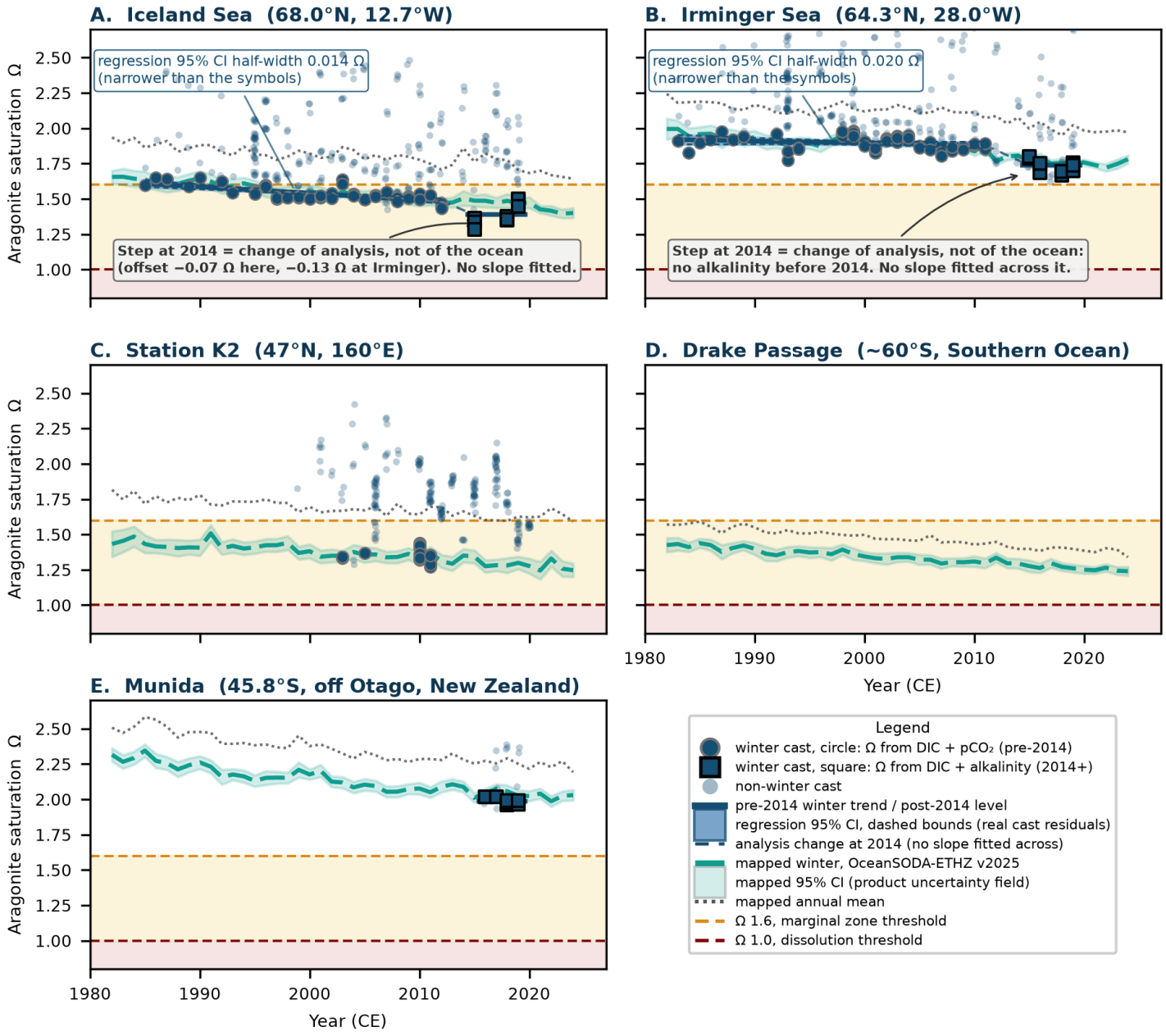


Figure 1

Figure 1: Measured winter surface aragonite saturation at five subpolar and high-latitude sites

Panels show the Iceland Sea (A), the Irminger Sea (B), Station K2 (C), Drake Passage (D) and Munida (E). Circles show discrete winter casts before 2014, computed from dissolved inorganic carbon with the partial pressure of carbon dioxide; squares show casts from 2014 onwards, computed from dissolved inorganic carbon with measured alkalinity. Dark blue shows the winter regression before 2014 with its 95% confidence band and the mean level after 2014; no slope is fitted across 2014 because the change of input pair introduces an analytical offset. Teal dashed lines show the mapped OceanSODA-ETHZ winter mean with its 95% band [5], grey dotted lines show the mapped annual mean, and faint small

circles show casts outside winter. Winter is January to March in the Northern Hemisphere and July to September in the Southern Hemisphere. Drake Passage has no sustained discrete record, so only the mapped product is shown there. Methods and cast counts are given in Additional file 1, Note S1.

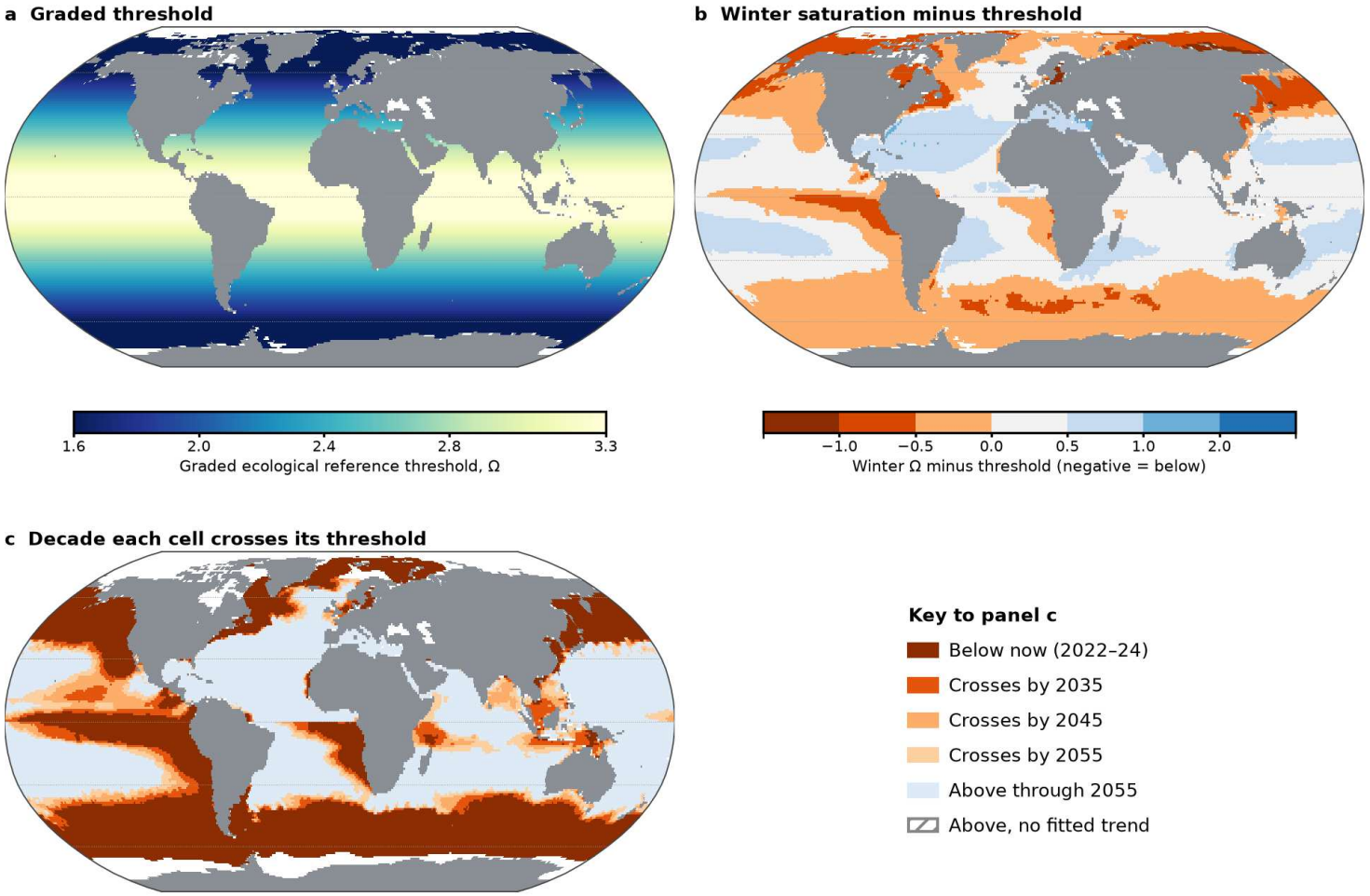


Figure 2

Figure 2: Winter surface aragonite saturation compared with a graded ecological reference threshold

(a) The threshold falls linearly with absolute latitude from Ω 3.3 equatorward of 10° [20] to Ω 1.6 poleward of 60° [17–19]. (b) Winter saturation in the 2022–2024 winters minus the threshold; orange-to-brown cells are below threshold. (c) The decade in which each cell crosses its threshold on its own 1982–2024 winter trend [5], from below threshold now (darkest) to above threshold through 2055 (palest); cells above threshold with no fitted trend are hatched. Winter is February in the Northern Hemisphere and August in the Southern Hemisphere. Land is grey; cells without winter data (mainly sea ice) are white; where adjacent polar water is measured, its median Ω is about 1.4, even in summer. Projections are linear and should be read as indicative beyond about 2045.

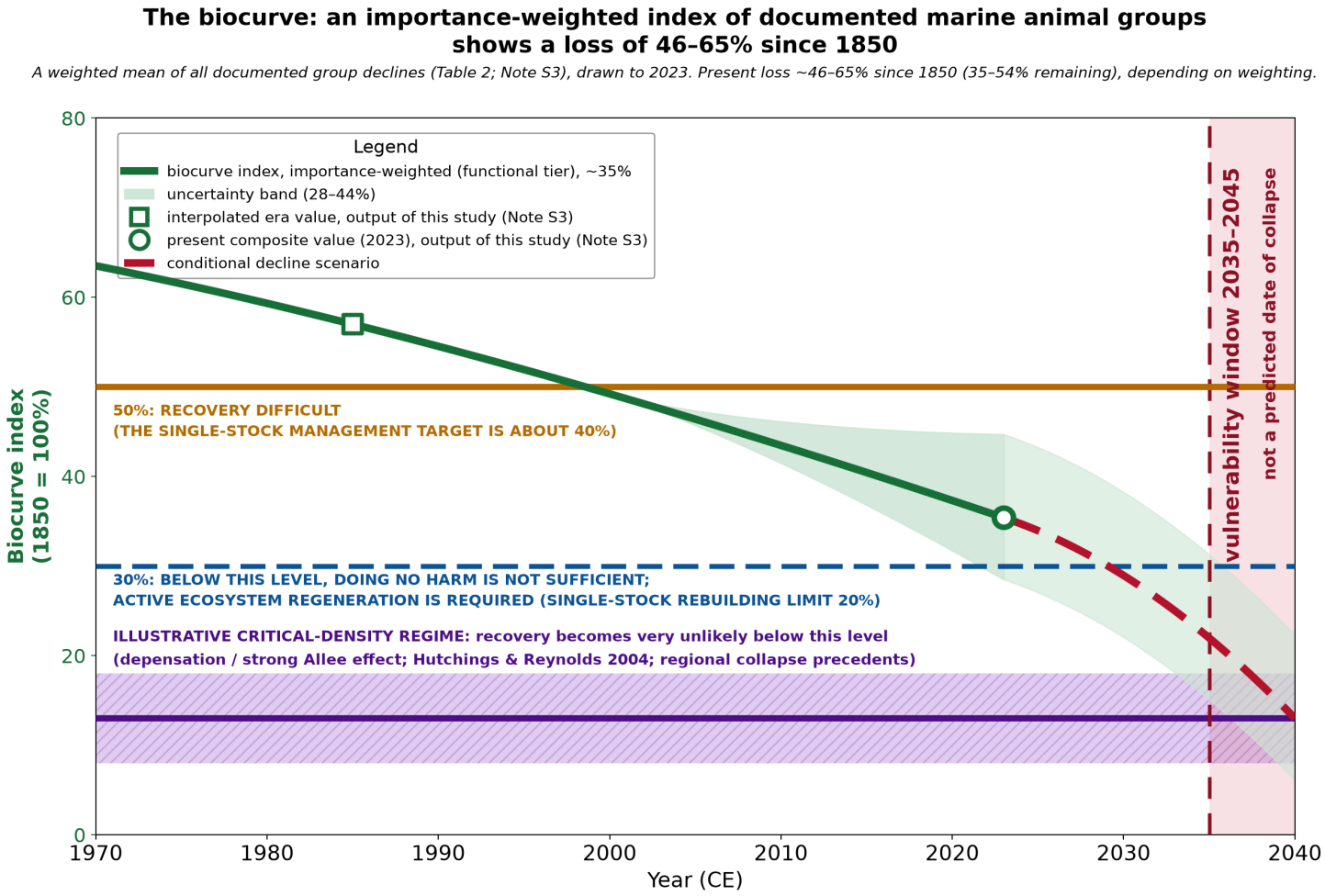


Figure 3

Figure 3: The biocurve, an index of documented declines in marine animal life since 1850

The index is expressed relative to its 1850 level of 100% and is drawn to about 2023 (Table 2; Additional file 1, Note S3) and is shown from 1970. The solid amber line at 50% and the dashed blue line at 30% are reference levels drawn by analogy with single-stock fisheries management, in which the target is the biomass at maximum sustainable yield, of the order of 40% of the unfished level, a stock below 20% must have a rebuilding plan, and one below 10% is considered for closure [133]; collapsed stocks rarely recover without such a plan [120, 121], and recovery becomes slower and less predictable the longer and deeper the depletion [134]. Below the first line, recovery becomes difficult, and below the second, doing no harm is not sufficient, and active ecosystem regeneration is required. The index is a composite of many groups, so the analogy is illustrative, and both lines are set above the single-stock values because the index includes slow-recovering groups. The curve is an interpretive synthesis rather than a census: the open square marks the interpolated value for 1985, the open circle marks the present composite, and the shaded band carries the uncertainty of the importance weighting. The red line is a scenario rather than a projection: it shows the direction that the theory of Section 4.6 permits if present pressures continue, and its entry into the illustrative critical-density regime (purple) is a stated choice rather than a computed value. The vertical band

from 2035 to 2045 marks the period in which 39 to 45% of the mapped ocean is projected to be below its winter threshold (Figure 2); it is not a predicted date of collapse.

Supplementary Files

This is a list of supplementary files associated with this preprint. Click to download.

- 7Additionalfile1.docx